Mechanics of Materials 173 (2022) 104420

Contents lists available at ScienceDirect

Mechanics of Materials

journal homepage: www.elsevier.com/locate/mecmat

Research paper

Homogenization of electrets with ellipsoidal microstructure and pathways for designing piezoelectricity in soft materials

Amir Hossein Rahmati [a], Liping Liu [b], Pradeep Sharma [a,c,*]

[a] Department of Mechanical Engineering, University of Houston, TX, USA
[b] Department of Mathematics and Mechanical and Aerospace Engineering, Rutgers University, NJ 08854, USA
[c] Department of Physics, University of Houston, Houston, TX 77204, USA

ARTICLE INFO

Keywords:
Electromechanical coupling
Electrets
Soft matter

ABSTRACT

True piezoelectricity in soft materials is rare if not virtually non-existent. This impedes applications where both large deformation and a strong electromechanical coupling are desirable e.g. soft robotics, biomedical sensors and actuators, a class of energy harvesting devices among others. The widely used soft dielectric elastomers rely on the electrostatic Maxwell stress effect for electromechanical coupling — a *one-way* quadratic effect that requires extremely large voltage for actuation and does not allow for the facile conversion of mechanical deformation into electricity. Prior research has shown that embedding (and stabilizing) immobile charges or dipoles in soft matter i.e. creating so-called *electrets*, can lead to an emergent piezoelectric effect. In this work, using a recently developed homogenization theory for soft electret materials, we derive closed-form expressions to design soft apparently piezoelectric materials with an ellipsoidal microstructure. Specifically, we determine both effective longitudinal (d_{33}) and transverse (d_{31}) piezoelectric coefficients of the material and study the impact of the material properties on these two coefficients. Conventional electrets exhibit a rather weak d_{31}, which is quite disadvantageous for applications where flexure is important (e.g. energy harvesting). Either an elastic, or a dielectric contrast is essential for the emergence of piezoelectricity in electrets and, depending on the microstructural details, these two effects can either strengthen or diminish the other. Our results indicate that the microstructure and material properties which lead to an optimum d_{33} effect are different from the conditions underlying the optimal d_{31} response. The maximum d_{31} effect is observed in electrets where the inclusions are mechanically harder but dielectrically softer than the matrix material. Finally, we find that a significantly large d_{33} piezoelectric response is possible for spheroid inclusion microstructures with large aspect ratios.

1. Introduction

Soft materials are capable of large deformation and thus enable applications in the area of soft robotics (Trivedi et al., 2008), stretchable and wearable electronics (Dong et al., 2020; Rogers et al., 2010; Ghadi et al., 2019; Kammoun et al., 2016), flexible sensors and actuators (Rafsanjani et al., 2018; Lim et al., 2020) and biocompatible devices (Cianchetti et al., 2018; Kim et al., 2012). A key imperative in the design of soft materials is to induce a mechanical response when subjected to a suitable stimuli e.g. electrical or magnetic fields, pH, temperature among others. Many applications of soft materials require a piezoelectric effect — a two way *linear* coupling between electric field and mechanical deformation. However, non-trivial piezoelectricity exists only in a rather limited number of materials. The typical piezoelectric materials (usually crystalline) are hard, brittle and are ill-suited for some of the aforementioned applications. The electromechanical coupling in soft dielectrics is limited to the electrostatic Maxwell stress effect (or alternatively electrostriction).[1] Due to electrostriction, all dielectric material deform in response to an applied electric field (Newnham et al., 1997). However, this effect is rather weak so hard dielectrics barely exhibit any discernible deformation. While soft materials like dielectric elastomers are well-able to exploit this form of electromechanical coupling, we note that electrostriction is a nonlinear (quadratic) coupling where the deformation scales as the square of the imposed electric field. This implies that deformation does not reverse if the imposed electric field is reversed. In addition, electrostriction is a one-way coupling i.e. the material deforms in

* Corresponding author at: Department of Mechanical Engineering, University of Houston, TX, USA.
E-mail addresses: Liu.liping@rutgers.edu (L. Liu), psharma@uh.edu (P. Sharma).

[1] In what follows, we will use these terms interchangeably and simply refer to both as "electrostriction". For a more subtle discussion regarding their distinction, see Zhao and Suo (2008).

https://doi.org/10.1016/j.mechmat.2022.104420
Received 3 June 2022; Received in revised form 22 July 2022; Accepted 23 July 2022
Available online 17 August 2022

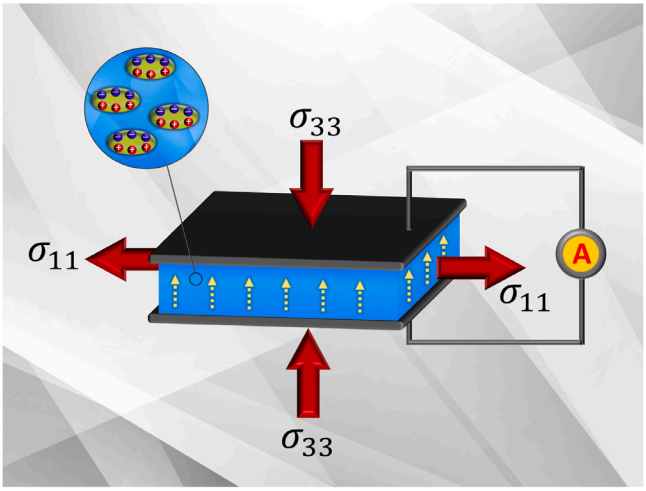

Fig. 1. Longitudinal and transverse piezoelectric effects in electret materials composed of a matrix and embedded inclusions. Existence of electric charges with opposite signs on the surface of inclusions lead to the existence of a nonzero residual polarization inside the material (shown schematically with arrows). Electric field generated as a result of loading σ_{33} is referred as d_{33} effect and electric field generated as a result of loading σ_{11} is referred as d_{31} effect.

response to an electric field but the applied deformation does not generate an electric field. Finally, significantly large electrical fields are necessary to induce actuation.

There appear to be two approaches to engineer a piezoelectric-like behavior in otherwise non-piezoelectric soft materials: (i) exploitation of the phenomenon of flexoelectricity (Yudin and Tagantsev, 2013; Zubko et al., 2013; Krichen and Sharma, 2016), and (ii) embedding immobile charges and dipoles in materials thus creating so-called electrets. Discussion of flexoelectricity is beyond the scope of this work and we refer the reader to several original works (Sharma et al., 2007; Mocci et al., 2021; Zhang et al., 2021; Majdoub et al., 2008, 2009; Mbarki et al., 2014; Mohammadi et al., 2014; Wang et al., 2019; Grasinger et al., 2021; Abdollahi et al., 2019) and review articles (Tagantsev and Yudin, 2016; Krichen and Sharma, 2016; Deng et al., 2017, 2020; Nguyen et al., 2013; Zhuang et al., 2022) for further information. The exploitation of electrets as materials that can mimic piezoelectrics began in earnest in the eighties (Sessler, 1980) when researchers created soft foamy polymers with charges and dipoles trapped on void surfaces (Sessler and Hillenbrand, 1999; Neugschwandtner et al., 2000; Zhang et al., 2004). Piezoelectric coefficient as large as 1200 pC/N (almost 6 times PZT) has been reported for such materials (Hillenbrand and Sessler, 2008; Bauer et al., 2003).

Electret materials have been subject of experimental research for several decades (Kacprzyk et al., 1997; Neugschwandtner et al., 2000; Hillenbrand and Sessler, 2000; Wen et al., 2019) including, recent, in the context of 2D materials (Apte et al., 2020). They have found applications in microphones (Sessler and West, 1966), sensors (Gong et al., 2019), data storage (Cheng et al., 2018) and energy harvesting (Suzuki et al., 2010; Boland et al., 2003)–in short, where-ever piezoelectrics are used. At this point of development, electret materials with large surface charge densities can be easily fabricated (Kashiwagi et al., 2011). In addition, there have been several successful attempts for improving charge stability in electrets — a key issue impeding their practical application. For example, Luo et al. (2021) developed a spray coating method for charge deposition to improve long term charge stability.

Recently, a few theoretical studies have also provided insights into the design of electromechanical coupling in electret materials. Deng et al. (2014a,b) presented a continuum model to explain the emergence of piezoelectricity in simple 1-D layered electret structures. They were able to interpret existing experimental results in which a large longitudinal piezoelectric effect (so-called d_{33} effect) is observed in electret materials(see Fig. 1 for explanation of longitudinal and transverse piezoelectric effect). We remark that the transverse piezoelectric coefficient is singularly important for applications (so-called d_{31} effect) such as energy harvesting and in general, for both sensing and actuation where flexure (the most facile deformation mode) is important. However, conventional electrets exhibit a large d_{33} but not d_{31}. Rahmati et al. (2019) created a model to explain the reason for small transverse piezoelectric effect in charged polymer foams and proposed simple beam-based designs to improve this feature. Recently, Liu and Sharma (2018) presented a comprehensive theory of homogenization of electret materials.[2] Works prior to this reference focussed on simple boundary value problems to illustrate apparent piezoelectricity. In the work of Liu and Sharma, they were able to rigorously predict a true bulk piezoelectric effect and the conditions necessary to achieve this. Specifically, they also presented some explicit results for effective piezoelectric properties of some simple specific microstructures (e.g. laminates). In addition, they showed that either elastic mismatch or dielectric mismatch in electrets is essential for the emergence of an apparent piezoelectric effect. We remark that electrets have also been used to create other forms of multifunctional materials such as magnetoelectrics (Alameh et al., 2015; Tan et al., 2021), pyroelectric/electrocaloric materials (Darbaniyan et al., 2019) or understand biological phenomena (Darbaniyan et al., 2021; Torbati et al., 2022).

Despite the work on electrets so far, there remain several unanswered questions about the emergent piezoelectric effect:

- Elastic heterogeneity is essential for the emergence of piezoelectricity in electrets however it is unclear how the interplay of elastic properties impact the average piezoelectric response.
- Although a large d_{33} piezoelectric coefficient has been achieved in electrets, the d_{31} effect is usually quite small (Neugschwandtner et al., 2001; Rahmati et al., 2019). What design strategy may be employed to improve d_{31} coefficient in electrets?
- Liu and Sharma (2018) argue that either elastic or dielectric mismatch must be present in electrets for apparent piezoelectricity. What is the interplay between dielectric and elastic mismatch in terms of tuning the effective response of electrets?
- Existing theoretical work have typically analyzed one-dimensional (or quasi-one-dimensional) electrets. While these studies have been insightful, little is known about how a 3D dimensional microstructure could impact the effective piezoelectric response of electrets.

In this work, using the broad homogenization theoretical framework of Liu and Sharma (2018), we analyze soft electret materials with ellipsoidal inclusions. The ellipsoidal microstructure is versatile enough for us to comment on issues such as the role of aspect ratio of heterogeneities and address the questions and observations highlighted in the preceding section.[3]

2. A summary of homogenization theory for electrets

In this section, we present a very brief summary of the homogenization theory for electrets presented by Liu and Sharma (2018). The essential relations required to determine effective properties of electrets are listed in this section without presenting the details. We refer the reader to Liu and Sharma (2018) for further information.

[2] See also Lefevre and Lopez-Pamies (2017) for a different take on the homogenization of electrets.

[3] We remark that several related aspects, which while of significant interest, are beyond the scope of this paper, e.g. (i) stability and bifurcation of soft electrets (Yang et al., 2017), (ii) use of enriched continuum theories (Sharma and Dasgupta, 2002; Sharma, 2004; Lakes, 2016, 2015).

2.1. Energy formulation

We follow the exact same notation as used by Liu and Sharma (2018). The deformable elastic body of the electret in the reference configuration is denoted by $\mathcal{D}$. The deformation $\mathbf{y}$ and the nominal polarization $\mathbf{p}$ are two independent thermodynamic variables which describe the state of the system $(\mathbf{y}, \mathbf{p}) : \mathcal{D} \to \mathbb{R}^3 \times \mathbb{R}^3$. Material points in the reference configuration are denoted by $\mathbf{x}$. Gradient in the reference (resp. current) configuration is denoted by ∇ ($\nabla_{\mathbf{y}}$). Also, deformation gradient tensor, Jacobian and the right Cauchy–Green deformation tensor are denoted by $\mathbf{F} = \nabla \mathbf{y}$, $J = \det\mathbf{F}$ and $\mathbf{C} = \mathbf{F}^T\mathbf{F}$, respectively. The electric potential is represented by $\xi : \mathcal{D} \to \mathbb{R}$. Dirichlet boundary condition has been applied to the whole boundary of the body $\partial\mathcal{D}$:

$$\xi = \xi_b \quad \text{on} \quad \partial\mathcal{D} \quad \text{and} \quad \mathbf{y} = \mathbf{x} + \mathbf{u}_b \quad \text{on} \quad \partial\mathcal{D}, \tag{1}$$

where ξ_b and $\mathbf{u}_b$ are, respectively, prescribed electric potential and displacement on the boundary. Following convention is used for inner products of tensors: for third order tensor $\mathbf{A}$ and second order tensor $\mathbf{B}$ we have $\mathbf{A} : \mathbf{B} = A_{ijk}B_{jk}\mathbf{e}_i$, for forth order tensors $\mathbf{A}$ and $\mathbf{B}$ we have $\mathbf{AB} = A_{ijkl}B_{klmn}(\mathbf{e}_i \otimes \mathbf{e}_j \otimes \mathbf{e}_m \otimes \mathbf{e}_n)$ and for second order tensor $\mathbf{A}$ and vector $\mathbf{a}$ we have $\mathbf{Aa} = A_{ij}a_j\mathbf{e}_i$.

The general form of the free energy of the system may be expressed as

$$F[\mathbf{y}, \mathbf{p}] = U[\mathbf{y}, \mathbf{p}] + \mathcal{E}^{\text{elect}}[\mathbf{y}, \mathbf{p}], \tag{2}$$

where $U[\mathbf{y}, \mathbf{p}]$ is the internal energy of the dielectric material. $\mathcal{E}^{\text{elect}}[\mathbf{y}, \mathbf{p}]$ is the electric energy and is given as (Liu, 2014)

$$\mathcal{E}^{\text{elect}}[\mathbf{y}, \mathbf{p}] = \int_{\mathcal{D}_{\mathbf{y}}} \frac{\epsilon_0}{2}|-\nabla_{\mathbf{y}}\xi|^2 + \int_{\partial\mathcal{D}_{\mathbf{y}}} \xi_b \mathbf{n}_{\mathbf{y}} \cdot (-\epsilon_0\nabla_{\mathbf{y}}\xi + \mathbf{p}/J), \tag{3}$$

where ϵ_0 and $\mathbf{n}_{\mathbf{y}}$ are electric permittivity of the vacuum and unit normal to the boundary in the current configuration, respectively. Also, $\mathcal{D}_{\mathbf{y}}$ denotes the body in the current configuration. The first term in Eq. (3) is the total electric energy associated with the electric field and the second term is the energy associated with boundary electrical devices. Substituting Eq. (3) into Eq. (2) and representing electric energy in the reference configuration, the free energy of the system can be written as

$$\begin{aligned} F[\mathbf{y}, \mathbf{p}] = &\int_{\mathcal{D}} \left[\Psi(\nabla\mathbf{y}, \mathbf{p}) + \frac{\epsilon_0}{2}\nabla\xi \cdot J\mathbf{C}^{-1}\nabla\xi\right] \mathrm{d}\mathbf{x} \\ + &\int_{\partial\mathcal{D}} \xi_b \mathbf{n} \cdot (-\epsilon_0 J\mathbf{C}^{-1}\nabla\xi + \mathbf{F}^{-1}\mathbf{p}), \end{aligned} \tag{4}$$

where $\Psi : \mathbb{R}^{3\times3} \times \mathbb{R}^3 \to \mathbb{R}$ is the internal energy density function and $\mathbf{n}$ is the unit normal to the boundary. The equilibrium state of the system is the state that minimizes free energy given in Eq. (4) and also satisfies the Maxwell's equations. The Maxwell's equations in the reference configuration can be expressed as

$$\nabla \cdot (-\epsilon_0 J\mathbf{C}^{-1}\nabla\xi + \mathbf{F}^{-1}\mathbf{p} + \mathbf{F}^{-1}\mathbf{p}^e) = \rho^e, \tag{5}$$

where $\mathbf{p}^e$ and ρ^e are external electric dipoles and charges, respectively.[4] In order to obtain a linearized theory, we restrict ourselves to the regime of small deformation and moderately small electric field:

$$\nabla\mathbf{u} \sim \varepsilon \ll 1, \qquad \mathbf{p} \sim \varepsilon^{1/2}, \tag{6}$$

where $\mathbf{u}(\mathbf{x}) = \mathbf{y}(\mathbf{x}) - \mathbf{x}$ is the displacement. We introduce the reciprocal dielectric susceptibility tensors $\boldsymbol{\chi}$, the stiffness tensors $\mathbb{C}$ and the electrostriction tensor $\mathbb{M}$ as

$$\boldsymbol{\chi} = \frac{\partial^2\Psi}{\partial\mathbf{p}\partial\mathbf{p}}, \qquad \mathbb{C} = \frac{\partial^2\Psi}{\partial\mathbf{F}\partial\mathbf{F}}, \qquad \mathbb{M} = \frac{1}{2}\frac{\partial^3\Psi}{\partial\mathbf{F}\partial\mathbf{p}\partial\mathbf{p}}, \tag{7}$$

where all derivatives have been evaluated at $(\mathbf{F}, \mathbf{p}) = (\mathbf{I}, \mathbf{0})$. We refer the reader to Liu and Sharma (2018) for the discussion on implication of the principles of frame indifference and material symmetries on these tensors. For isotropic materials $\mathbb{C}$ and $\mathbb{M}$ can be written as

$$\mathbb{C}_{ijkl} = \mu(\delta_{ik}\delta_{jl} + \delta_{il}\delta_{jk}) + \lambda\delta_{ij}\delta_{kl}, \tag{8}$$

$$\mathbb{M}_{ijkl} = m_\mu(\delta_{ik}\delta_{jl} + \delta_{il}\delta_{jk}) + m_\lambda\delta_{ij}\delta_{kl}, \tag{9}$$

where λ and μ are Lame constant and shear modulus of the material and m_μ and m_λ are the two electrostriction related parameters. Using the Taylor series expansion and the scaling given in the Eq. (6), the free energy can be decomposed (Tian, 2008; Tian et al., 2012; Liu, 2014):

$$F[\mathbf{y}, \mathbf{p}] = F^{(0)} + F^{(1)} + F^{(2)} + o(\varepsilon^2), \tag{10}$$

where $F^{(0)} := F[\mathbf{y} = \mathbf{x}, \mathbf{p} = \mathbf{0}]$ and

$$\begin{aligned} F^{(1)}[\mathbf{p}] = &\int_{\mathcal{D}} \left[\frac{1}{2}\mathbf{p} \cdot \boldsymbol{\chi}\mathbf{p} + \frac{\epsilon_0}{2}|\nabla\xi|^2\right] \mathrm{d}\mathbf{x} \\ + &\int_{\partial\mathcal{D}} \left[\xi_b\mathbf{n} \cdot (-\epsilon_0\nabla\xi + \mathbf{p} + \mathbf{p}^e)\right] \mathrm{d}\mathbf{x} \sim \varepsilon, \end{aligned} \tag{11}$$

$$\begin{aligned} F^{(2)}[\mathbf{u}, \mathbf{p}] = &\int_{\mathcal{D}} \left[\frac{1}{2}\nabla\mathbf{u} \cdot \mathbb{C}\nabla\mathbf{u} + \nabla\mathbf{u} \cdot \mathbb{M}(\mathbf{p} \otimes \mathbf{p})\right. \\ + &\left.\nabla\mathbf{u} \cdot \boldsymbol{\sigma}_{\text{MW}}\right] \mathrm{d}\mathbf{x} \sim \varepsilon^2, \end{aligned} \tag{12}$$

where $\boldsymbol{\sigma}_{\text{MW}}$ is given as

$$\boldsymbol{\sigma}_{\text{MW}} = -\frac{\epsilon_0}{2}|\nabla\xi|^2\mathbf{I} + \epsilon_0\nabla\xi \otimes \nabla\xi - \nabla\xi \otimes \mathbf{p}. \tag{13}$$

We identify the forth order electrostrictive coupling tensor $\mathbb{A}$ as

$$\begin{aligned} \mathbb{A}_{ijkl} = &(\mathbb{M})_{ijk'l'}(\boldsymbol{\chi}^{-1})_{kk'}(\boldsymbol{\chi}^{-1})_{ll'} \\ + &\frac{\epsilon_0}{2}\mathbb{T}_{ijkl} + \frac{1}{2}[\delta_{ik}(\boldsymbol{\chi}^{-1})_{jl} + \delta_{il}(\boldsymbol{\chi}^{-1})_{jk}], \end{aligned} \tag{14}$$

where the fourth-order tensor $\mathbb{T} : \mathbb{R}^{3\times3} \to \mathbb{R}^{3\times3}$ is given as

$$\begin{aligned} &\mathbb{T}\mathbf{F} = \mathbf{F} + \mathbf{F}^T - (\mathrm{Tr}\mathbf{F})\mathbf{I} \qquad \forall\mathbf{F} \in \mathbb{R}^{3\times3}, \\ &\mathbb{T}_{ijkl} = \delta_{ik}\delta_{jl} + \delta_{il}\delta_{jk} - \delta_{ij}\delta_{kl}. \end{aligned} \tag{15}$$

We identify the dielectric tensor as $\boldsymbol{\epsilon} = \epsilon_0\mathbf{I} + \boldsymbol{\chi}^{-1}$. The dielectric tensor and the electrostrictive coupling tensor for isotropic materials are expressed as $\boldsymbol{\epsilon} = \epsilon\mathbf{I}$ and $\mathbb{A} = \frac{\epsilon}{2}\mathbb{T}$. We can use first of Eq. (11) to write equilibrium equations of the system in terms of electric potential and displacement:

$$\nabla \cdot (-\boldsymbol{\epsilon}\nabla\xi + \mathbf{p}^e) = \rho^e \qquad \text{in} \quad \mathcal{D} \tag{16}$$

$$\nabla \cdot (\mathbb{C}\nabla\mathbf{u} + \mathbb{A}(\nabla\xi \otimes \nabla\xi)) = \mathbf{0} \qquad \text{in} \quad \mathcal{D} \tag{17}$$

2.2. Effective properties of the electrets

We assume electrostatic body of the electret $\mathcal{D}$ has a periodic microstructure (see Fig. 2). The rescaled unit cell (or RVE) of the composite is denoted by $Y = (0, 1)^3 \subset \mathcal{D}$. We identify fast variables $\widetilde{\mathbf{x}} = \mathbf{x}/\delta$, where δ is the scaling parameter δ reflects the fine microstructure of the composite as compared with the macroscopic length-scale of the domain $\mathcal{D}$. For a domain $\mathcal{D}$, $\fint_{\mathcal{D}}$ denotes the average of the integrand on $\mathcal{D}$. Dielectric tensor, stiffness tensor and electrostrictive coupling tensor are assumed to be Y-periodic functions:

$$\left(\boldsymbol{\epsilon}^{(\delta)}(\mathbf{x}), \mathbb{C}^{(\delta)}(\mathbf{x}), \mathbb{A}^{(\delta)}(\mathbf{x})\right) = \left(\boldsymbol{\epsilon}_{\#}\left(\widetilde{\mathbf{x}}\right), \mathbb{C}_{\#}\left(\widetilde{\mathbf{x}}\right), \mathbb{A}_{\#}\left(\widetilde{\mathbf{x}}\right)\right), \tag{18}$$

where $\widetilde{\mathbf{x}} = \frac{\mathbf{x}}{\delta}$ is the fast variable.

2.2.1. Effective stiffness and effective electric permittivity tensor

We identify the effective electric permittivity tensor $\boldsymbol{\epsilon}^{\text{eff}}$, the effective stiffness tensor $\mathbb{C}^{\text{eff}}$ and the effective electrostrictive tensor $\mathbb{A}^{\text{eff}}$ as (Tian et al., 2012; Tian, 2008)

$$\boldsymbol{\epsilon}^{\text{eff}}\bar{\mathbf{e}} = \fint_Y [\boldsymbol{\epsilon}_{\#}(\widetilde{\mathbf{x}})(-\nabla\xi_{\bar{\mathbf{e}}})] \qquad \text{for} \quad \bar{\mathbf{e}} \in \mathbb{R}^3, \tag{19}$$

$$\mathbb{C}^{\text{eff}}\bar{\mathbf{H}} = \fint_Y [\mathbb{C}_{\#}(\widetilde{\mathbf{x}})(\nabla\mathbf{u}_{\bar{\mathbf{H}}})] \qquad \text{for} \quad \bar{\mathbf{H}} \in \mathbb{R}^{3\times3}, \tag{20}$$

[4] We remark that efficient approaches to solve the electrostatic Gauss equation in all of space are discussed in Ref. Yang and Dayal (2011).

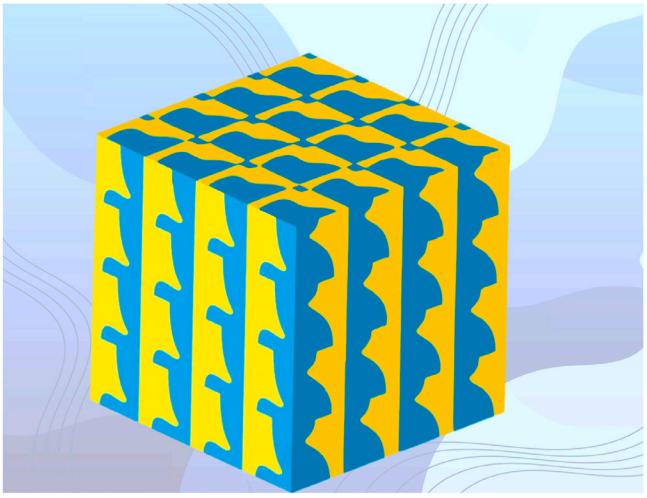

Fig. 2. A schematic of a periodic microstructure. The color in each unit cell could be heterogeneities or external, immobile positive and negative charges.

$$\bar{\mathbf{H}} \cdot \mathbb{A}^{\text{eff}}(\bar{\mathbf{e}} \otimes \bar{\mathbf{e}}) = \fint_Y [\nabla \mathbf{u}_{\bar{\mathbf{H}}} \cdot \mathbb{A}_{\#}(\widetilde{\mathbf{x}})(\nabla \xi_{\bar{\mathbf{e}}} \otimes \nabla \xi_{\bar{\mathbf{e}}})] \quad \text{for} \quad (\bar{\mathbf{e}}, \bar{\mathbf{H}}) \in \mathbb{R}^3 \times \mathbb{R}^{3\times 3}, \tag{21}$$

where the electric potential $\xi_{\bar{\mathbf{e}}} \in \mathcal{P}_{\bar{\mathbf{e}}}$ and $\mathbf{u}_{\bar{\mathbf{H}}} \in \mathcal{U}_{\bar{\mathbf{H}}}$ satisfy unit cell equilibrium equations

$$\text{div}[\epsilon_{\#}(\widetilde{\mathbf{x}})(-\nabla \xi_{\bar{\mathbf{e}}})] = 0, \tag{22}$$

$$\text{div}[\mathbb{C}_{\#}(\widetilde{\mathbf{x}})(\nabla \mathbf{u}_{\bar{\mathbf{H}}})] = \mathbf{0}. \tag{23}$$

Also, admissible spaces $\mathcal{P}_{\bar{\mathbf{e}}}$ and $\mathcal{U}_{\bar{\mathbf{H}}}$ are defined as

$$\mathcal{P}_{\bar{\mathbf{e}}} \equiv \left\{ \xi : -\fint_Y \nabla \xi = \bar{\mathbf{e}} \quad \text{and} \quad \nabla \xi \quad \text{is Y-periodic} \right\} \tag{24}$$

$$\mathcal{U}_{\bar{\mathbf{H}}} \equiv \left\{ \mathbf{u} : \fint_Y \nabla \mathbf{u} = \bar{\mathbf{H}} \quad \text{and} \quad \nabla \mathbf{u} \quad \text{is Y-periodic} \right\}. \tag{25}$$

2.2.2. Multiscale analysis and effective piezoelectric tensor

We represent microstructural distribution of external dipoles and charges by $(\mathbf{p}^{(\delta)}, \rho^{\delta})$. We assume a periodic distribution for external charges and dipoles inside the material:

$$(\mathbf{p}^{(\delta)}, \rho^{\delta}) = \left(\bar{\mathbf{p}} + \mathbf{p}_{\#}(\frac{\mathbf{x}}{\delta}), \bar{\rho} + \frac{1}{\delta}\rho_{\#}(\frac{\mathbf{x}}{\delta}) \right), \tag{26}$$

where $\mathbf{p}_{\#}$ and $\rho_{\#}$ are Y-periodic functions:

$$\fint_Y (\mathbf{p}_{\#}, \rho_{\#}) = 0. \tag{27}$$

Existence of external charges and/or dipoles will lead to a piezoelectric effect in electret materials. We use multiscale analysis based on the method of two-scale convergence (Cioranescu and Donato, 1999; Milton, 2002) in order to define the effective piezoelectric tensor. Using scaling discussed earlier, electrostatic problem is decoupled from elasticity. Thus, we perform multi-scale analysis on the electrostatic equilibrium equation first. The local electric field can be determined by solving

$$\begin{cases} \text{div}[-\epsilon^{(\delta)} \nabla \xi^{(\delta)} + \mathbf{p}^{(\delta)}] = \rho^{(\delta)} & \text{in} \quad D, \\ \xi^{(\delta)} = \xi_b & \text{on} \quad \partial D. \end{cases} \tag{28}$$

The goal of current theory is to analyze the behavior of the material in the limit $\delta \to 0$. Following the formal procedure of multiscale analysis, the solution to Eq. (28) is given as

$$\xi^{(\delta)}(\mathbf{x}) = \xi^{(0)}(\mathbf{x}, \widetilde{\mathbf{x}}) + \delta \xi^{(1)}(\mathbf{x}, \widetilde{\mathbf{x}}) + \cdots, \tag{29}$$

where $\widetilde{\mathbf{x}} \mapsto \xi^{(i)}(\mathbf{x}, \widetilde{\mathbf{x}})$ is Y-periodic for all i and $\fint_Y \xi^{(i)} = 0$ if $i \neq 0$. Using chain rule we can rewrite gradient and divergence operators as $\nabla \to \nabla_{\mathbf{x}} + \frac{1}{\delta}\nabla_{\widetilde{\mathbf{x}}}$ and $\text{div} \to \text{div}_{\mathbf{x}} + \frac{1}{\delta}\text{div}_{\widetilde{\mathbf{x}}}$. It can be proved that the first order of the solution (29) is independent of the fast variable $\widetilde{\mathbf{x}} = \frac{\mathbf{x}}{\delta}$ and can be determined from following equation

$$\begin{cases} \text{div}_{\mathbf{x}} \left(-\boldsymbol{\epsilon}^{\text{eff}} \nabla_{\mathbf{x}} \xi^{(0)} + \chi_D(\bar{\mathbf{p}} + \bar{\mathbf{d}}') \right) = \bar{\rho} & \text{in} \quad D, \\ \xi^{(0)} = \xi_b & \text{on} \quad \partial D, \end{cases} \tag{30}$$

where $\chi_D = 1$ on D and $\chi_D = 0$ otherwise. Also, $\bar{\mathbf{d}}'$ is defined as

$$\bar{\mathbf{d}}' = \fint_Y \boldsymbol{\epsilon}_{\#}(-\nabla_{\widetilde{\mathbf{x}}} \xi'), \tag{31}$$

and $\xi' \in \mathcal{P}_0$ and is a solution to the following equation

$$\text{div}_{\widetilde{\mathbf{x}}}[\epsilon_{\#}(\widetilde{\mathbf{x}})(-\nabla_{\widetilde{\mathbf{x}}} \xi') + \mathbf{p}_{\#}] = \rho_{\#} \qquad \text{in Y}. \tag{32}$$

The Eq. (32) is the key equation in the calculation of the effective piezoelectric tensor; which we will use later. Also, ξ' can be related to $\xi^{(1)}$ defined in the Eq. (29). For more details, reader is referred to the Liu and Sharma (2018).

Next, we can analyze the elasticity problem using a similar procedure as we used for the electrostatic problem. The mechanical equilibrium equation is expressed as

$$\begin{cases} \text{div}[\mathbb{C}^{(\delta)} \nabla \mathbf{u}^{(\delta)} + \mathbb{A}^{(\delta)} \nabla \xi^{(\delta)} \otimes \xi^{(\delta)}] = 0, & \text{in} \quad D \\ \mathbf{u}^{(\delta)} = \mathbf{u}_b & \text{on} \quad \partial D \end{cases} \tag{33}$$

The solution to above equation can be written as

$$\mathbf{u}^{(\delta)}(\mathbf{x}) = \mathbf{u}^{(0)}(\mathbf{x}, \widetilde{\mathbf{x}}) + \delta \mathbf{u}^{(1)}(\mathbf{x}, \widetilde{\mathbf{x}}) + \cdots, \tag{34}$$

where $\mathbf{u}^{(i)}(\mathbf{x}, \widetilde{\mathbf{x}})$ is Y-periodic for all i and $\fint_Y \mathbf{u}^{(i)} = 0$ if $i \neq 0$. We identify $\mathbf{u}'_1 \in \mathcal{U}_0$ which satisfies

$$\text{div}_{\widetilde{\mathbf{x}}} \left[\mathbb{C}_{\#}(\widetilde{\mathbf{x}}) \nabla_{\widetilde{\mathbf{x}}} \mathbf{u}'_1 + 2\mathbb{A}_{\#}(\widetilde{\mathbf{x}})(\nabla_{\widetilde{\mathbf{x}}} \xi' \otimes \nabla_{\widetilde{\mathbf{x}}} \xi_{\bar{\mathbf{e}}}) \right] = 0. \tag{35}$$

It can be shown that the macroscopic displacement $\mathbf{u}^{(0)}$ is independent of the fast variable ($\mathbf{u}^{(0)} = \mathbf{u}^{(0)}(\mathbf{x})$). The boundary value problem for the macroscopic displacement $\mathbf{u}^{(0)}$ is given as

$$\begin{cases} \text{div}_{\mathbf{x}} \boldsymbol{\sigma} = 0, & \text{in} \quad D, \\ \mathbf{u}^{(0)} = \mathbf{u}_b & \text{on} \quad \partial D, \end{cases} \tag{36}$$

where the total stress $\boldsymbol{\sigma}$ is defined as

$$\boldsymbol{\sigma} \equiv \mathbb{C}^{\text{eff}} \nabla_{\mathbf{x}} \mathbf{u}^{(0)} - \mathbb{B}^{\text{eff}} \nabla_{\mathbf{x}} \xi^{(0)} + \mathbb{A}^{\text{eff}}(\nabla_{\mathbf{x}} \xi^{(0)} \otimes \nabla_{\mathbf{x}} \xi^{(0)}) + \boldsymbol{\sigma}^0. \tag{37}$$

The second order tensor $\boldsymbol{\sigma}^0$ is independent of the average electric field and strain. The definition of the tensor $\boldsymbol{\sigma}^0$ is available in Liu and Sharma (2018). Also, $\mathbb{B}^{\text{eff}}$ is the effective piezoelectric tensor and is defined as

$$\mathbb{B}^{\text{eff}} \bar{\mathbf{e}} = \fint_Y [\mathbb{C}_{\#}(\widetilde{\mathbf{x}}) \nabla_{\widetilde{\mathbf{x}}} \mathbf{u}'_1 + 2\mathbb{A}_{\#}(\widetilde{\mathbf{x}})(\nabla_{\widetilde{\mathbf{x}}} \xi' \otimes \nabla_{\widetilde{\mathbf{x}}} \xi_{\bar{\mathbf{e}}})]. \tag{38}$$

3. Effective piezoelectric properties of an electret with ellipsoidal inclusion

In this section, we use the theory presented earlier to obtain the effective piezoelectric properties of an electret with ellipsoidal inclusion. The unit cell of the material is shown in Fig. 3. We assume both matrix and inclusion are homogeneous isotropic materials. We identify the unit cell by Y and the inclusion is represented by Ω. We denote the stiffness tensor for the matrix (resp. inclusion) by $\mathbb{C}^m$ (resp. $\mathbb{C}^p$). Also, we represent the electric permittivity the tensor of the matrix and inclusion with $\boldsymbol{\epsilon}_m = \epsilon_m \mathbf{I}$ and $\boldsymbol{\epsilon}_p = \epsilon_p \mathbf{I}$, respectively. We assume that there exist a nonzero uniform polarization $\mathbf{p}_s$ inside the inclusion.

In order to determine the piezoelectric tensor for the ellipsoidal microstructure, first we need to solve electrostatic Eqs. (32) and (22). Introducing the variable χ_p (resp. χ_m) such that $\chi_p = 1$ (resp. $\chi_m = 1$)

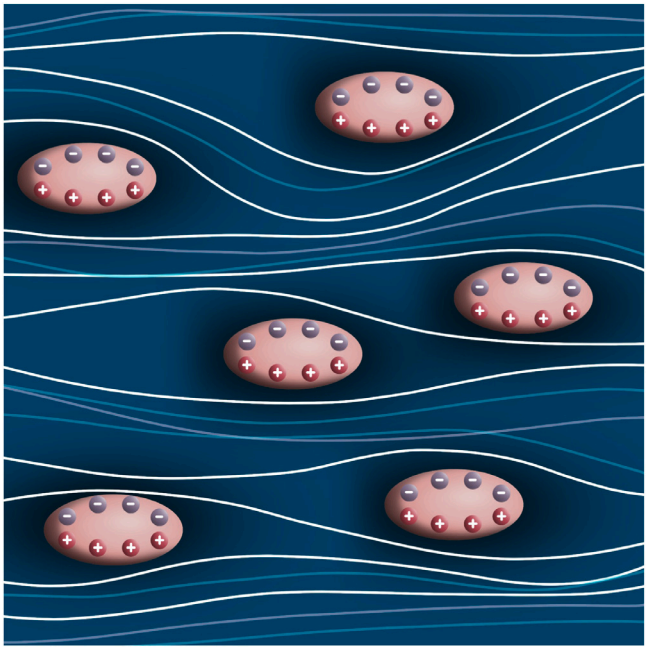

Fig. 3. The schematic of the electret material with ellipsoidal inclusions.

for $x \in \Omega$ (resp. $x \in Y/\Omega$) and $\chi_p = 0$ (resp. $\chi_m = 0$) otherwise, we rewrite these two equations as

$$\mathrm{div}[-(\epsilon_m\chi_m + \epsilon_p\chi_p)\nabla\xi' + \mathbf{p}_s\chi_p] = 0 \qquad \text{in} \quad Y, \tag{39}$$

$$\mathrm{div}[-(\epsilon_m\chi_m + \epsilon_p\chi_p)\nabla\xi_{\bar{\mathbf{e}}}] = 0 \qquad \text{in} \quad Y, \tag{40}$$

where

$$\fint_Y \nabla\xi' = \mathbf{0}, \qquad \fint_Y \nabla\xi_{\bar{\mathbf{e}}} = -\bar{\mathbf{e}}. \tag{41}$$

After we solve electrostatic equations (39) and (40), we need to solve elasticity equation (35) which can be rewritten as

$$\mathrm{div}\left((\mathbb{C}^p\chi_p + \mathbb{C}^m\chi_m)\nabla\mathbf{u}' + \boldsymbol{\sigma}^{(e)}\right) = \mathbf{0}, \tag{42}$$

where here we have dropped the subscript 1 from $\mathbf{u}'_1$ for brevity. Also, we identify $\boldsymbol{\sigma}^{(e)}$ as

$$\boldsymbol{\sigma}^{(e)} = \epsilon_{\#}\mathbb{T}(\nabla\xi' \otimes \nabla\xi_{\bar{\mathbf{e}}}). \tag{43}$$

Effective dielectric tensor is defined as

$$\boldsymbol{\epsilon}^{\mathrm{eff}}\bar{\mathbf{e}} = -\fint_Y \epsilon_{\#}\nabla\xi_{\bar{\mathbf{e}}} \tag{44}$$

Once we have determined ξ', $\xi_{\bar{\mathbf{e}}}$ and $\mathbf{u}'$ we can obtain the effective piezoelectric tensor using

$$\mathbb{B}^{\mathrm{eff}}\mathbf{e} = \fint_Y \left[\mathbb{C}_{\#}\nabla\mathbf{u}' + \boldsymbol{\sigma}^{(\bar{\mathbf{e}})}\right]. \tag{45}$$

3.1. Solution to electrostatic problems

The solution for Eqs. (39) and (40) is obtained by solving the following equation for the ellipsoidal inclusion:

$$\mathrm{div}(-\nabla\hat{\psi}_{\mathbf{m}} + \mathbf{m}\chi_p) = 0 \tag{46}$$

where $\mathbf{m} \in \mathbb{R}^3$ is a constant vector and $\nabla\hat{\psi}_{\mathbf{m}} \to \mathbf{0}$ at the infinity. In order to obtain solution for Eq. (46), we express $\hat{\psi}_{\mathbf{m}}$ and $\mathbf{m}$ in terms of their Fourier transforms $\bar{\psi}_{\mathbf{m}}$ and $\bar{\mathbf{m}}$, respectively:

$$\hat{\psi}_{\mathbf{m}} = \int_{\mathbb{R}^3} \bar{\psi}_{\mathbf{m}}(\mathbf{k})\exp(i\mathbf{k}\cdot\mathbf{x})\,\mathrm{d}\mathbf{k}, \tag{47}$$

$$\mathbf{m} = \int_{\mathbb{R}^3} \bar{\mathbf{m}}(\mathbf{k})\exp(i\mathbf{k}\cdot\mathbf{x})\,\mathrm{d}\mathbf{k}. \tag{48}$$

Substituting Eqs. (48) and (47) into (46), we have

$$\int_{\mathbb{R}^3} \left(\bar{\psi}_{\mathbf{m}}k_ik_i + i\bar{m}_jk_j\right)\exp(i\mathbf{k}\cdot\mathbf{x}) = 0. \tag{49}$$

Thus, $\bar{\psi}_{\mathbf{m}}$ can be determined as

$$\bar{\psi}_{\mathbf{m}} = -\frac{ik_j\bar{m}_j}{k_ik_i}. \tag{50}$$

Now consider the Green's function $G(\mathbf{x}-\mathbf{x}')$ as

$$G(\mathbf{x}-\mathbf{x}') = \frac{1}{4\pi}\frac{1}{|\mathbf{x}-\mathbf{x}'|}. \tag{51}$$

The Green's function $G(\mathbf{x}-\mathbf{x}')$ is expressed in terms of its Fourier transform $\bar{G}(\mathbf{k})$ as (Hiroshi and Minoru, 1986; Li and Wang, 2008)

$$G(\mathbf{x}-\mathbf{x}') = \int_{\mathbb{R}^3} \bar{G}(\mathbf{k})\exp\left(i\mathbf{k}\cdot(\mathbf{x}-\mathbf{x}')\right)\mathrm{d}\mathbf{k}, \tag{52}$$

where

$$\bar{G}(\mathbf{k}) = \frac{1}{(2\pi)^3}\frac{1}{k_ik_i}. \tag{53}$$

Substituting Eq. (50) into Eq. (47) and using Eq. (53) we have:

$$\hat{\psi_{\mathbf{m}}} = -(2\pi)^3\int_{\mathbb{R}^3} \overline{G_{,j}}\bar{m}_j\exp(i\mathbf{k}\cdot\mathbf{x})\,\mathrm{d}\mathbf{k}, \tag{54}$$

where $\overline{G_{,j}}$ is the Fourier transform of $G_{,j}$ where throughout this paper subscript "," means partial derivative. For example, $G_{,j} = \frac{\partial G}{\partial x_j}$. Using convolution theorem we can rewrite (54) as (Li and Wang, 2008)

$$\hat{\psi_{\mathbf{m}}} = -\int_\Omega G_{,j}(\mathbf{x}-\mathbf{x}')m_j\mathrm{d}\mathbf{x}'. \tag{55}$$

We identify function $\Phi(\mathbf{x}) = \int_\Omega \frac{1}{|\mathbf{x}-\mathbf{x}'|}\mathrm{d}\mathbf{x}'$. For constant $\mathbf{m}$ and using Eqs. (55) and (51), we express $\nabla\hat{\psi_{\mathbf{m}}}$ as

$$\nabla\hat{\psi_{\mathbf{m}}} = \mathbf{Q}\mathbf{m} \qquad \text{for} \quad x \in Y, \tag{56}$$

where $Q_{ij} = -\frac{1}{4\pi}\Phi_{,ij}$. We introduce following elliptic integrals:

$$I(s) = 2\pi a_1a_2a_3\int_s^\infty \frac{\mathrm{d}s}{\Delta(s)}, \tag{57}$$

$$I_i(s) = 2\pi a_1a_2a_3\int_s^\infty \frac{\mathrm{d}s}{(a_i^2+s)\Delta(s)}, \tag{58}$$

$$I_{ij}(s) = 2\pi a_1a_2a_3\int_s^\infty \frac{\mathrm{d}s}{(a_i^2+s)(a_j^2+s)\Delta(s)}, \tag{59}$$

where

$$\Delta(s) = \sqrt{(a_1^2+s)(a_2^2+s)(a_3^2+s)}. \tag{60}$$

Components of Q_{ij} for elliptical inclusion with principal semi-axes a_1, a_2 and a_3 can be determined as (Hiroshi and Minoru, 1986; Mura, 2013)

$$Q_{ij} = Q_{ij}^- = \frac{1}{4\pi}\left(\delta_{ij}I_I(0)\right) \qquad \text{for} \quad x \in \Omega, \tag{61}$$

$$Q_{ij}(\mathbf{x}) = Q_{ij}^+ = \frac{1}{4\pi}\left(\delta_{ij}I_I(s) - x_iI_{I,J}\right) \qquad \text{for} \quad x \in \mathbb{R}^3/\Omega, \tag{62}$$

where the following summation convention has been used: repeated lower case indices are summed up from 1 to 3; upper case indices take on the same numbers as the corresponding lower case ones but are not summed. As well known, for elliptical inclusions in an in finite linear media, the electric field inside the inclusion is a constant (Liu, 2008; Eshelby, 1957). Also, the elliptical integrals (57), (58) and (59) can be explicitly determined for several kinds of ellipsoid. Here, in this paper, we consider a prolate spheroid with radii a_1, a_2 and a_3 along x_1, x_2 and x_3 directions, respectively (see Fig. 3). For prolate spheroid with $a_2 = a_3 < a_1$, the components of $\mathbf{Q}$ tensor for interior points ($\mathbf{Q}^-$) can be determined substituting Eq. (57) into Eq. (61) :

$$\mathbf{Q}^- = Q_{11}^-\mathbf{e}_1 \otimes \mathbf{e}_1 + Q_{22}^-\mathbf{e}_2 \otimes \mathbf{e}_2 + Q_{33}^-\mathbf{e}_3 \otimes \mathbf{e}_3, \tag{63}$$

where $\{\mathbf{e}_1, \mathbf{e}_2, \mathbf{e}_3\}$ represents the coordinate system and

$$Q_{33}^- = Q_{22}^- =$$

$$\frac{a_3^2 a_1}{2(a_1^2-a_3^2)^{3/2}} \times \left[\frac{a_1}{a_3}\left(\frac{a_1^2}{a_3^2}-1\right)^{1/2} - \cosh^{-1}\frac{a_1}{a_3} \right], \tag{64}$$

$$Q_{11}^{-} = 1 - 2Q_{22}^{-}. \tag{65}$$

Also, using jump conditions, the solution on the outer surface of the inclusion can be determined in terms of the solution inside the inclusion as

$$\nabla\hat{\psi}_{\mathbf{m}}|_{\partial\Omega^+} = \mathbf{Q}^{-}\mathbf{m} - (\mathbf{n}\cdot\mathbf{m})\mathbf{n}. \tag{66}$$

Having the solution (56) for Eq. (46), we can determine $\nabla\xi'$ and $\nabla\xi_{\bar{\mathbf{e}}}$. We introduce $\mathbf{m}_1$ and $\mathbf{m}_2$ as

$$\mathbf{m}_1 = [\epsilon_m\mathbf{I} + (\epsilon_p-\epsilon_m)\mathbf{Q}^{-}]^{-1}\mathbf{p}_s, \tag{67}$$

$$\mathbf{m}_2 = (\epsilon_p-\epsilon_m)[\epsilon_m\mathbf{I} + (\epsilon_p-\epsilon_m)\mathbf{Q}^{-}]^{-1}\bar{\mathbf{e}}. \tag{68}$$

By setting $\mathbf{m}=\mathbf{m}_1$ and $\mathbf{m}=\mathbf{m}_2$ in Eq. (46), the electric fields $\nabla\xi'$ and $\nabla\xi_{\bar{\mathbf{e}}}$ can be determined respectively. The solution to Eqs. (39) and (40) is given as

$$\nabla\xi' = \nabla\hat{\psi}_{\mathbf{m}_1}, \tag{69}$$

$$\nabla\xi_{\bar{\mathbf{e}}} = -\bar{\mathbf{e}} + \nabla\hat{\psi}_{\mathbf{m}_2}. \tag{70}$$

In order to determine piezoelectric coefficient defined in the Eq. (45), we need to calculate $\fint_Y \boldsymbol{\sigma}^{(\bar{\mathbf{e}})}$. We have

$$\fint_Y \boldsymbol{\sigma}^{(\bar{\mathbf{e}})} = (1-\theta)\fint_{Y/\Omega}\boldsymbol{\sigma}^{(\bar{\mathbf{e}})} + \theta\fint_{\Omega}\boldsymbol{\sigma}^{(\bar{\mathbf{e}})}, \tag{71}$$

The second term on the right hand side of Eq. (71) can be simply determined substituting Eqs. (56), (69) and (70) into Eq. (71):

$$\theta\fint_{\Omega}\boldsymbol{\sigma}^{(\bar{\mathbf{e}})} = -\theta\epsilon_p\mathbb{T}\left(\mathbf{Q}^{-}\mathbf{m}_1\otimes\bar{\mathbf{e}}\right) + \theta\mathbb{T}\epsilon_p\left(\mathbf{Q}^{-}\mathbf{m}_1\otimes\mathbf{Q}^{-}\mathbf{m}_2\right). \tag{72}$$

As the values of the components of the tensor $\mathbf{Q}$ are not constant for the points located outside the inclusion, it is difficult to determine the first integral on the right hand side of the Eq. (71). Obtaining explicit relations for the effective piezoelectric tensor will not be possible unless we express all volume integrals in terms of the solutions obtained for electric fields inside the inclusion. Therefore, from Eq. (41), we write

$$\fint_{Y/\Omega}\nabla\xi' = \frac{-\theta}{1-\theta}\fint_{\Omega}\nabla\xi' = \frac{-\theta}{1-\theta}\mathbf{Q}^{-}\mathbf{m}_1, \tag{73}$$

$$\fint_{Y/\Omega}\nabla\xi_{\bar{\mathbf{e}}} = \frac{1}{1-\theta}\left(-\bar{\mathbf{e}} - \theta\fint_{\Omega}\nabla\xi_{\bar{\mathbf{e}}}\right) = -\bar{\mathbf{e}} - \frac{\theta}{1-\theta}\mathbf{Q}^{-}\mathbf{m}_2. \tag{74}$$

We introduce $\nabla\xi_{\bar{\mathbf{e}}}^{(1)}$ and $\nabla\xi'^{(1)}$ such that

$$\nabla\xi_{\bar{\mathbf{e}}} = \left(\fint_{Y/\Omega}\nabla\xi_{\bar{\mathbf{e}}}\right) + \nabla\xi_{\bar{\mathbf{e}}}^{(1)} \qquad \text{for} \quad \mathbf{x}\in Y/\Omega, \tag{75}$$

$$\nabla\xi' = \left(\fint_{Y/\Omega}\nabla\xi'\right) + \nabla\xi'^{(1)} \qquad \text{for} \quad \mathbf{x}\in Y/\Omega, \tag{76}$$

where

$$\fint_{Y/\Omega}\nabla\xi'^{(1)} = \mathbf{0}, \qquad \fint_{Y/\Omega}\nabla\xi_{\bar{\mathbf{e}}}^{(1)} = \mathbf{0}. \tag{77}$$

Substituting Eqs. (75) and (76) into Eq. (71), we have

$$\begin{aligned}(1-\theta)\fint_{Y/\Omega}\boldsymbol{\sigma}^{(\bar{\mathbf{e}})} &= (1-\theta)\epsilon_m\fint_{Y/\Omega}\mathbb{T}\left(\nabla\xi'^{(1)}\otimes\nabla\xi_{\bar{\mathbf{e}}}^{(1)}\right) + \\ &(1-\theta)\epsilon_m\mathbb{T}\left(\left[\fint_{Y/\Omega}\nabla\xi'\right]\otimes\left[\fint_{Y/\Omega}\nabla\xi_{\bar{\mathbf{e}}}\right]\right).\end{aligned} \tag{78}$$

We can ignore the first term on the right hand side of the Eq. (78) and rewrite this equation as

$$\begin{aligned}(1-\theta)\fint_{Y/\Omega}\boldsymbol{\sigma}^{(\bar{\mathbf{e}})} &\approx \\ (1-\theta)\epsilon_m\mathbb{T}&\left(\left[\fint_{Y/\Omega}\nabla\xi'\right]\otimes\left[\fint_{Y/\Omega}\nabla\xi_{\bar{\mathbf{e}}}\right]\right).\end{aligned} \tag{79}$$

Substituting (79), (72), (74) and (73) into (71), we have

$$\begin{aligned}\fint_Y\boldsymbol{\sigma}^{(\bar{\mathbf{e}})} &= \theta(\epsilon_m-\epsilon_p)\mathbb{T}\left(\mathbf{Q}^{-}\mathbf{m}_1\otimes\bar{\mathbf{e}}\right) \\ &+ \theta\left(\frac{\theta}{1-\theta}\epsilon_m+\epsilon_p\right)\mathbb{T}\left(\mathbf{Q}^{-}\mathbf{m}_1\otimes\mathbf{Q}^{-}\mathbf{m}_2\right)\end{aligned} \tag{80}$$

Eq. (80) can be expressed in terms of $\boldsymbol{\epsilon}^{\text{eff}}$, ϵ_m, ϵ_p and θ. In order to do so, we rewrite Eq. (44) as

$$-\fint_Y \epsilon_{\#}\nabla\xi_{\bar{\mathbf{e}}} = -\fint_Y\left(\epsilon_m - \chi_p(\epsilon_m-\epsilon_p)\right)\nabla\xi_{\bar{\mathbf{e}}} = \boldsymbol{\epsilon}^{\text{eff}}\bar{\mathbf{e}}. \tag{81}$$

Therefore, from (56), (69) and (70) we have

$$\mathbf{Q}^{-}\mathbf{m}_2 = \frac{1}{\theta(\epsilon_m-\epsilon_p)}\left(\boldsymbol{\epsilon}^{\text{eff}} - \epsilon_m\mathbf{I} + \theta(\epsilon_m-\epsilon_p)\mathbf{I}\right)\bar{\mathbf{e}}, \tag{82}$$

$$\mathbf{Q}^{-}\mathbf{m}_1 = -\frac{1}{\theta(\epsilon_m-\epsilon_p)^2}\left(\boldsymbol{\epsilon}^{\text{eff}} - \epsilon_m\mathbf{I} + \theta(\epsilon_m-\epsilon_p)\mathbf{I}\right)\mathbf{p}_s. \tag{83}$$

Substituting Eqs. (82) and (83) into (80), the average stress $\fint_Y\boldsymbol{\sigma}^{(\bar{\mathbf{e}})}$ is expressed in terms of $\boldsymbol{\epsilon}^{\text{eff}}$, ϵ_m, ϵ_p and θ:

$$\begin{aligned}\fint_Y\boldsymbol{\sigma}^{(\bar{\mathbf{e}})} &= -\frac{1}{\epsilon_m-\epsilon_p}\mathbb{T}\left[(\boldsymbol{\epsilon}^{*}\mathbf{p}_s)\otimes\bar{\mathbf{e}}\right] \\ &- \left(\frac{\theta}{1-\theta}\epsilon_m+\epsilon_p\right)\frac{1}{\theta(\epsilon_m-\epsilon_p)^3}\mathbb{T}\left\{(\boldsymbol{\epsilon}^{*}\mathbf{p}_s)\otimes(\boldsymbol{\epsilon}^{*}\bar{\mathbf{e}})\right\},\end{aligned} \tag{84}$$

where

$$\boldsymbol{\epsilon}^{*} = \left(\boldsymbol{\epsilon}^{\text{eff}} - \epsilon_m\mathbf{I} + \theta(\epsilon_m-\epsilon_p)\mathbf{I}\right). \tag{85}$$

3.2. Elasticity problem

Next, we consider the elastic unit-cell problem (42). The source term $\boldsymbol{\sigma}^{(\bar{\mathbf{e}})}$ physically can be interpreted as an eigenstress induced by electric fields. It clear that the eigenstress $\boldsymbol{\sigma}^{(\bar{\mathbf{e}})}$ is uniform inside Ω since $\nabla\xi'$ and $\nabla\xi_{\bar{\mathbf{e}}}$ are both uniform on Ω. Further, since $\xi'_{,jj}=0$ and $\xi_{\bar{\mathbf{e}}_{,jj}}=0$ in $\mathbb{R}^3\setminus\Omega$, we find that

$$\begin{aligned}\sigma_{ij,j}^{(\bar{\mathbf{e}})} =& \epsilon\xi'_{,ij}(\xi_{\bar{\mathbf{e}}})_{,j}\epsilon\xi'_{,j}(\xi_{\bar{\mathbf{e}}})_{,ij} \\ &- \epsilon\xi'_{,jij}(\xi_{\bar{\mathbf{e}}})_{,j} - \epsilon\xi'_{,j}(\xi_{\bar{\mathbf{e}}})_{,ji} = 0 \qquad \text{in} \quad \mathbb{R}^3\setminus\Omega.\end{aligned} \tag{86}$$

Therefore, Maxwell stress is divergence free if restricted to interior or exterior of Ω. Jump on the Maxwell stress over the surface of ellipsoid can be determined substituting Eqs. (66), (69), (70) to (43):

$$\mathbf{t}^{(\bar{\mathbf{e}})} := [\![\boldsymbol{\sigma}^{(\bar{\mathbf{e}})}]\!]\mathbf{n} = \boldsymbol{\sigma}^{*}\mathbf{n} + p^{*}\mathbf{n}, \tag{87}$$

where

$$\begin{aligned}\boldsymbol{\sigma}^{*} &= (\epsilon_m-\epsilon_p)\mathbb{T}\left[(\mathbf{Q}^{-}\mathbf{m}_1)\otimes(-\bar{\mathbf{e}}+\mathbf{Q}^{-}\mathbf{m}_2)\right] \\ &- \epsilon_m\left[(-\bar{\mathbf{e}}+\mathbf{Q}^{-}\mathbf{m}_2)\otimes\mathbf{m}_1 + (\mathbf{Q}^{-}\mathbf{m}_1\otimes\mathbf{m}_2)\right],\end{aligned} \tag{88}$$

and

$$p^{*} = \epsilon_m(\mathbf{m}_1\cdot\mathbf{n})(\mathbf{m}_2\cdot\mathbf{n}). \tag{89}$$

If there exist both elastic and dielectric contrast, we need to solve Eq. (42). We rewrite this equilibrium equation as

$$\text{div}\left(\mathbb{C}^m\nabla\mathbf{u}' - \chi_p(\mathbb{C}^m-\mathbb{C}^p)\nabla\mathbf{u}' + \boldsymbol{\sigma}^{(\bar{\mathbf{e}})}\right) = \mathbf{0}. \tag{90}$$

Using Eq. (87), the solution to equilibrium equation (90) is given as (Sharma, 2004)

$$\begin{aligned}\mathbf{u}'(\mathbf{x}) = -\int_{\Omega}&\left[\nabla_{\mathbf{x}}\mathbf{G}^{\text{elast}}(\mathbf{x}-\mathbf{x}') : \right. \\ &\left.\left(\boldsymbol{\sigma}^{*} + (\mathbb{C}^m-\mathbb{C}^p)\left(\nabla_{\mathbf{x}}\mathbf{u}'(\mathbf{x})\right)\right)\right]\text{d}\mathbf{x}' \\ &+ \int_{\partial\Omega}[\mathbf{G}^{\text{elast}}(\mathbf{x}-\mathbf{x}')\mathbf{n}^{*}(\mathbf{x}')p^{*}]\text{d}\mathbf{x}',\end{aligned} \tag{91}$$

where $\mathbf{G}^{\text{elast}}(\mathbf{x}-\mathbf{x}')$ is the elasticity greens function for isotropic materials and is given as

$$\mathbf{G}^{\text{elast}}(\mathbf{x}-\mathbf{x}') = \frac{1}{16\pi\mu_m(1-\nu_m)|\mathbf{x}-\mathbf{x}'|}\times \left((3-4\nu_m)\delta_{ij} + \frac{(x_i-x_i')(x_j-x_j')}{|\mathbf{x}-\mathbf{x}'|^2}\right)(\mathbf{e}_i\otimes\mathbf{e}_j), \tag{92}$$

where μ_m and ν_m are shear modulus and Poisson's ratio of the matrix material. It is not easily possible to solve Eq. (91) for $\mathbf{u}'$ analytically. This is because existence of the term containing surface integral. This problem is equivalent of the conventional inclusion problem with nonuniform eigenstrain. In order to simplify this equation, we replace p^* with $\langle p^*\rangle = \frac{1}{S}\int_{\partial\Omega} p^* \mathrm{d}S$, where S is the surface area of the inclusion. Therefore, we identify $\boldsymbol{\Sigma}^* = (\boldsymbol{\sigma}^* + \langle p^*\rangle\mathbf{I})$ and write Eq. (87) as

$$\mathbf{t}^{(\bar{\boldsymbol{\epsilon}})} \approx \boldsymbol{\Sigma}^*\mathbf{n} = \left[\boldsymbol{\sigma}^* + \epsilon_m\left((\mathbf{m}_1\otimes\mathbf{m}_2) : (\mathbb{N})\right)\right]\mathbf{n}, \tag{93}$$

where the tensor $\mathbb{N}$ is defined as

$$\mathbb{N} = \frac{1}{S}\int_{\partial\Omega}[n_i n_j \mathbf{e}_i\otimes\mathbf{e}_j]\mathrm{d}S. \tag{94}$$

For the ellipsoidal inclusion with principal semi-axes a_1, a_2 and a_3 aligned along $\mathbf{e}_1$, $\mathbf{e}_2$ and $\mathbf{e}_3$ directions, the components of $\mathbb{N}$ are determined as (Rosenkilde, 1967)

$$\mathbb{N} = \frac{1}{S}2\pi(a_1a_2a_3)^2\int_0^\infty \frac{\delta_{ij}(\mathbf{e}_i\otimes\mathbf{e}_j)}{(a_I^2+t^2)\Delta}\mathrm{d}t, \tag{95}$$

where summation convention is suppressed for upper case indices and

$$\Delta = \sqrt{(a_1^2+t^2)(a_2^2+t^2)(a_3^2+t^2)}. \tag{96}$$

For a prolate spheroid with $a_1 = a_2$ and $a_3 > a_1$, we have

$$\mathbb{N} = N_{11}\mathbf{e}_1\otimes\mathbf{e}_1 + N_{22}\mathbf{e}_2\otimes\mathbf{e}_2 + N_{33}\mathbf{e}_3\otimes\mathbf{e}_3, \tag{97}$$

where

$$N_{33} = N_{22} = \frac{2}{S}\pi(a_1a_2a_3)^2\times\frac{\sqrt{1-k^2}}{2a_3^4k^2}\times \left[\sqrt{1-k^2} - (1-2k^2)\frac{\sin^{-1}k}{k}\right], \tag{98}$$

$$N_{11} = \frac{2}{S}\pi(a_1a_2a_3)^2\times\frac{\sqrt{1-k^2}}{a_1^4k^2}\left[\frac{\sin^{-1}k}{k} - \sqrt{1-k^2}\right], \tag{99}$$

and $k^2 = 1-(\frac{a_3}{a_1})^2$. Therefore, substituting Eq. (93) into Eq. (90) we have

$$\mathrm{div}\left(\mathbb{C}^m\nabla\mathbf{u}' - \chi_p(\mathbb{C}^m-\mathbb{C}^p)\nabla\mathbf{u}' - \boldsymbol{\Sigma}^*\right) = \mathbf{0}. \tag{100}$$

The solution for (100) is given as

$$\mathbf{u}'(\mathbf{x}) = -\int_\Omega\left[\nabla_{\mathbf{x}}\mathbf{G}^{\text{elast}}(\mathbf{x}-\mathbf{x}') : \left(\boldsymbol{\Sigma}^* + (\mathbb{C}^m-\mathbb{C}^p)\left(\nabla_{\mathbf{x}}\mathbf{u}'(\mathbf{x})\right)\right)\right]\mathrm{d}\mathbf{x}'. \tag{101}$$

In order to obtain the solution of the Eq. (101), we define the fourth order auxiliary tensor $\mathbb{S}$ as

$$\mathbb{S} = -\frac{1}{2}(\mathbf{e}_i\otimes\mathbf{e}_n\otimes\mathbf{e}_j\otimes\mathbf{e}_p)\left(\int_\Omega\left[\frac{\partial^2 G_{ij}^{\text{elast}}(\mathbf{x}-\mathbf{x}')}{\partial x_p\partial x_n} + \frac{\partial^2 G_{nj}^{\text{elast}}(\mathbf{x}-\mathbf{x}')}{\partial x_p\partial x_i}\right]\mathrm{d}\mathbf{x}'\right). \tag{102}$$

The tensor $\mathbb{S}$ can be related to so-called Eshelby tensor $\mathbb{S}^{\text{E}}$ by $\mathbb{S}^{\text{E}} = \mathbb{S}\mathbb{C}$ or

$$(\mathbb{C}^{-1})_{qrmn}(\mathbb{S}^{\text{E}})_{ijmn} = \frac{1}{2}\left((\mathbb{S})_{ijqr} + (\mathbb{S})_{ijrq}\right). \tag{103}$$

It is obvious that tensor $\mathbb{S}$ does not satisfy one of the minor symmetries. Similar to the Eshelby tensor $\mathbb{S}^{\text{E}}$, the components of the auxiliary tensor $\mathbb{S}$ can be determined for ellipsoidal inclusion by substituting Eq. (92) into Eq. (102). Reader is referred to the textbooks Mura (2013) and Li and Wang (2008) for details of the integration of the relation (102) for elliptical inclusions. We have calculated the tensor $\mathbb{S}$ and listed its components in the Appendix. It should be mentioned that, throughout this paper, we define $\mathbb{F}^{-1}$ as the inverse of an arbitrary fourth order tensor $\mathbb{F}$ if $(\mathbb{F}^{-1})_{ijkl} = (\mathbb{F}^{-1})_{jikl} = (\mathbb{F}^{-1})_{ijlk}$ and $(\mathbb{F}^{-1})_{ijkl}(\mathbb{F})_{klmn}\mathcal{A}_{mn} = \mathcal{A}_{ij}$ for any symmetric $\mathcal{A}_{ij}$.

Substituting Eq. (102) in to Eq. (101), the linear strain $\boldsymbol{\epsilon}' = \frac{1}{2}(\nabla\mathbf{u}' + (\nabla\mathbf{u}')^T)$ can be written as

$$\boldsymbol{\epsilon}' = \mathbb{S}\left(\boldsymbol{\Sigma}^* + (\mathbb{C}^m-\mathbb{C}^p)\boldsymbol{\epsilon}'\right). \tag{104}$$

Using the definition given for the inverse of fourth order tensors, the strain $\boldsymbol{\epsilon}'$ is determined as

$$\boldsymbol{\epsilon}' = (\mathbb{C}^p-\mathbb{C}^m+\mathbb{S}^{-1})^{-1}\boldsymbol{\Sigma}^{\text{SYM}}, \tag{105}$$

where

$$\boldsymbol{\Sigma}^{\text{SYM}} = \frac{1}{2}\left(\boldsymbol{\Sigma}^* + (\boldsymbol{\Sigma}^*)^T\right) + \frac{1}{2}\mathbb{S}^{-1}\mathbb{S}\left(\boldsymbol{\Sigma}^* - (\boldsymbol{\Sigma}^*)^T\right). \tag{106}$$

3.3. Effective elastic and piezoelectric properties

In this section, we determine the effective stiffness tensor $\mathbb{C}^{\text{eff}}$ and the effective piezoelectric tensor $\mathbb{B}^{\text{eff}}$ for the material shown in Fig. 3. In order to determine effective stiffness tensor defined in the Eq. (20), we need to solve Eq. (23). The Eq. (23) can be written in following fashion

$$\mathrm{div}\left(\mathbb{C}^m\nabla\mathbf{u}_{\bar{\mathbf{H}}} - \chi_p(\mathbb{C}^m-\mathbb{C}^p)\nabla\mathbf{u}_{\bar{\mathbf{H}}}\right) = \mathbf{0}, \tag{107}$$

where $\fint_Y\nabla\mathbf{u}_{\bar{\mathbf{H}}} = \bar{\mathbf{H}}$. We define $\mathbf{u}'_{\bar{\mathbf{H}}}$ such that $\nabla\mathbf{u}'_{\bar{\mathbf{H}}} = \nabla\mathbf{u}_{\bar{\mathbf{H}}} - \bar{\mathbf{H}}$. Thus, from Eq. (107), $\nabla\mathbf{u}'_{\bar{\mathbf{H}}}$ can be determined solving following equation:

$$\mathrm{div}\left(\mathbb{C}_{\#}\nabla\mathbf{u}'_{\bar{\mathbf{H}}} - \chi_p(\mathbb{C}^m-\mathbb{C}^p)\bar{\mathbf{H}}\right) = \mathbf{0}. \tag{108}$$

As $\bar{\mathbf{H}}$ is arbitrary, we set $(\mathbb{C}^m-\mathbb{C}^p)\bar{\mathbf{H}} = \boldsymbol{\Sigma}^{\text{SYM}}$. Substituting this relation into Eq. (108) yields

$$\mathrm{div}\left(\mathbb{C}_{\#}\nabla\mathbf{u}'_{\bar{\mathbf{H}}} - \chi_p\boldsymbol{\Sigma}^{\text{SYM}}\right) = \mathbf{0}. \tag{109}$$

The solution to (109) is given as

$$\frac{1}{2}\left(\nabla\mathbf{u}'_{\bar{\mathbf{H}}} + \nabla\mathbf{u}'^T_{\bar{\mathbf{H}}}\right) = \left(\mathbb{C}^p-\mathbb{C}^m+\mathbb{S}^{-1}\right)^{-1}\boldsymbol{\Sigma}^{\text{SYM}}. \tag{110}$$

Substituting the solution (110) in to the definition (20), a linear equation for effective stiffness tensor is derived as

$$\mathbb{C}^{\text{eff}}\bar{\mathbf{H}} = \fint_Y\mathbb{C}_{\#}\nabla\mathbf{u}_{\bar{\mathbf{H}}} = \fint_Y[\mathbb{C}_{\#}(\nabla\mathbf{u}'_{\bar{\mathbf{H}}} + \bar{\mathbf{H}})] = \bar{\mathbb{C}}\bar{\mathbf{H}} + \theta(\mathbb{C}^p-\mathbb{C}^m)\left(\mathbb{C}^p-\mathbb{C}^m+\mathbb{S}^{-1}\right)^{-1}\boldsymbol{\Sigma}^{\text{SYM}}, \tag{111}$$

where $\bar{\mathbb{C}} = \fint_Y\mathbb{C}$. From Eq. (111), the effective stiffness tensor is determined as

$$\mathbb{C}^{\text{eff}} = \bar{\mathbb{C}} + \theta(\mathbb{C}^p-\mathbb{C}^m)\left(\mathbb{C}^p-\mathbb{C}^m+\mathbb{S}^{-1}\right)^{-1}(\mathbb{C}^m-\mathbb{C}^p). \tag{112}$$

Substituting Eq. (105) into Eq. (45), the effective piezoelectric tensor can be written as

$$\mathbb{B}^{\text{eff}}\mathbf{e} = \fint_Y\left[\boldsymbol{\sigma}^{(\bar{\boldsymbol{\epsilon}})}\right] + \theta\fint_\Omega[(\mathbb{C}^p-\mathbb{C}^m)\nabla\mathbf{u}'] = \fint_Y\left[\boldsymbol{\sigma}^{(\bar{\boldsymbol{\epsilon}})}\right] + \theta(\mathbb{C}^p-\mathbb{C}^m)\left(\mathbb{C}^p-\mathbb{C}^m+\mathbb{S}^{-1}\right)^{-1}\boldsymbol{\Sigma}^{\text{SYM}}. \tag{113}$$

From Eq. (112) we have

$$\mathbb{B}^{\text{eff}}\mathbf{e} = = \fint_Y\left[\boldsymbol{\sigma}^{(\bar{\boldsymbol{\epsilon}})}\right] + (\mathbb{C}^{\text{eff}}-\bar{\mathbb{C}})(\mathbb{C}^m-\mathbb{C}^p)^{-1}\boldsymbol{\Sigma}^{\text{SYM}}. \tag{114}$$

Substituting Eq. (84) into (114), we obtain a linear set of equations which can be trivially solved to determine each component of the piezoelectric tensor $\mathbb{B}^{\text{eff}}$

$$\begin{aligned}\mathbb{B}^{\text{eff}}\mathbf{e} &= (\mathbb{C}^{\text{eff}} - \bar{\mathbb{C}})(\mathbb{C}^{m} - \mathbb{C}^{p})^{-1}\boldsymbol{\Sigma}^{\text{SYM}} \\ &- \frac{1}{\epsilon_m - \epsilon_p}\mathbb{T}\left[(\boldsymbol{\epsilon}^{*}\mathbf{p}_s)\otimes\bar{\mathbf{e}}\right] \\ &- \left(\frac{\theta}{1-\theta}\epsilon_m + \epsilon_p\right)\frac{1}{\theta(\epsilon_m-\epsilon_p)^3}\mathbb{T}\left\{(\boldsymbol{\epsilon}^{*}\mathbf{p}_s)\otimes(\boldsymbol{\epsilon}^{*}\bar{\mathbf{e}})\right\}.\end{aligned} \tag{115}$$

The Eq. (115) gives us a linear set of equations which can simply be solved to determine each component of the piezoelectric tensor $\mathbb{B}^{\text{eff}}$. The effective piezoelectric tensor depends on the effective electric permittivity tensor $\boldsymbol{\epsilon}^{\text{eff}}$ and effective stiffness tensor $\mathbb{C}^{\text{eff}}$ which can be determined using Eqs. (82) and (112), respectively. It is clear from Eq. (115) that the effective piezoelectric tensor linearly depends on the residual polarization $\mathbf{p}_s$. Also, from Eqs. (80) and (113), it is obvious that existence of elastic mismatch or dielectric mismatch is necessary condition to have a non-zero piezoelectric coefficient. The effective piezoelectric tensor $\mathbb{B}^{\text{eff}}$ relates electric field to stress and vice versa (see the relation (37)). We can define third order piezoelectric tensor $^{\text{eff}}$ which can be used to relate electric field to strain and vice versa. The piezoelectric tensor $\mathbf{d}^{\text{eff}}$ is defined as

$$-(\mathbb{C})^{\text{eff}}_{ijkl}(\mathbf{d}^{\text{eff}})_{mkl} = (\mathbb{B}^{\text{eff}})_{ijm} \tag{116}$$

or

$$(\mathbf{d}^{\text{eff}})_{mij} = -((\mathbb{C}^{\text{eff}})^{-1})_{ijkl}(\mathbb{B}^{\text{eff}})_{klm}. \tag{117}$$

In what follows, we will use contracted notation and denote d_{333}, d_{311}, d_{111} and d_{133} by d_{33}, d_{31}, d_{11} and d_{13}, respectively.

4. Results and discussion

In the presentation of our numerical results, unless otherwise stated we have set $\epsilon_m = 2.35\epsilon_0$, $\mu_m = 2.35\epsilon_0$ and $\mu_m = 1$ MPa, $\theta = 0.05$ and $a_1 = 5a_3$. Also, we assume that the inclusions are softer than the matrix with $\mu_m = 10^3\mu_p$ and $\nu_m = \nu_p$. We remark that typical experiments have been on void inclusions and since softness is an important element, the large elastic contrast we have chosen is physically relevant. In addition, we assume the inclusion has the polarization $\mathbf{p}_s = p_s\mathbf{e}_3$. We will change all these material properties and investigate the effects of each one of them on the effective piezoelectric coefficients of the material and draw pertinent insights regarding the questions posed in the Introduction.

In Fig. 4, we investigate the effect of the direction of polarization inside the material on the effective piezoelectric coefficients. We have set

$$\mathbf{p}_s = p_s\left(\cos(\alpha)\mathbf{e}_3 + \sin(\alpha)\mathbf{e}_1\right), \tag{118}$$

and plotted different piezoelectric coefficients with respect to the angle α. As evident, the d_{31} and d_{33} coefficients are maximized if the polarization is along the $\mathbf{e}_3$ direction. The d_{31} and d_{33} decreases as the polarization direction rotates from $\mathbf{e}_3$ direction toward $\mathbf{e}_1$ direction and these coefficients become zero when residual polarization is perpendicular to the $\mathbf{e}_3$ direction. This result implies that if the polarization is along $\mathbf{e}_3$ direction and if we apply an external electric field along $\mathbf{e}_1$ direction, we will not observe any piezoelectric effect and the material will behave similar to a conventional dielectric material. A similar results is reported for d_{11} and d_{13} piezoelectric coefficients where these two coefficients are zero at $\mathbf{p}_s = \pm p_s\mathbf{e}_3$ and they peak at $\mathbf{p}_s = \pm p_s\mathbf{e}_1$.

In addition, Fig. 4 shows that d_{33} (resp. d_{11}) piezoelectric coefficient is always greater than d_{31} (resp. d_{13}) for all values of α. This implies that the when an electric field is applied along the polarization direction of the material, the first order deformation observed along the polarization direction is always greater than the first order deformation observed along the direction perpendicular to polarization direction of the material. For the rest of this paper we set $\mathbf{p}_s = p_s\mathbf{e}_3$ and focus on d_{33} and d_{31} coefficients.

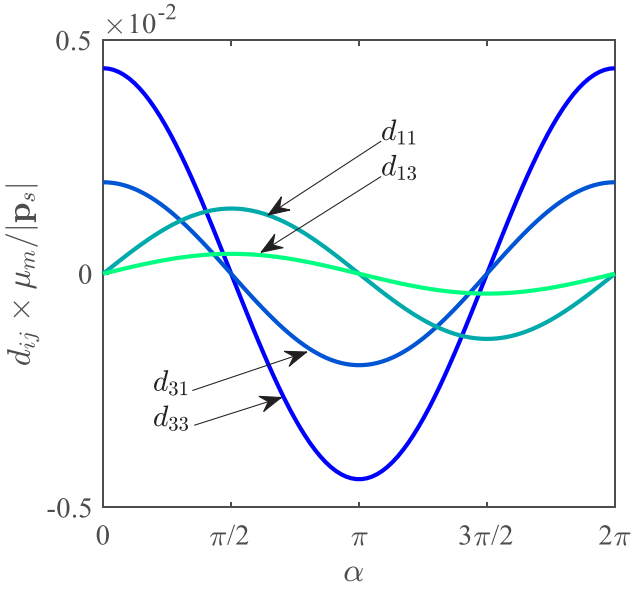

Fig. 4. Rotation of preexisting dipole and its effect on effective dimensionless piezoelectric coefficients of a composite material with ellipsoidal inclusions.

Fig. 5 show the variation of the effective piezoelectric coefficients with the ratio of inclusion shear modulus over matrix shear modulus ($\frac{\mu_p}{\mu_m}$) for different ratios of materials electric permittivity $\frac{\epsilon_p}{\epsilon_m}$. We have set the matrix electric permittivity to $\epsilon = 2.35\epsilon_0$ which is equivalent to polypropylene (PP) electric permittivity (Qu and Yu, 2011) and plotted piezoelectric coefficients. Note that the electric permittivity of the inclusion cannot be less than vacuum electric permittivity and the minimum possible value for electric permittivity ratio is $\frac{\epsilon_p}{\epsilon_m} = 1/2.35 \approx 0.5$. Thus, we have plotted piezoelectric coefficients for $0.5 \leq \frac{\epsilon_p}{\epsilon_m} \leq 2$. We will separately study the effect of electric permittivity ratio in due course. Figs. 5(a) and 5(b) show that in the absence of dielectric mismatch ($\frac{\epsilon_p}{\epsilon_m} = 1$) and elastic mismatch ($\frac{\epsilon_p}{\epsilon_m} = 1$) both piezoelectric coefficients d_{31} and d_{33} are zero (as expected) and as the ratio $\frac{\epsilon_p}{\epsilon_m}$ increases to the values greater than one or decreases to the value less than one, the magnitude of the piezoelectric effect increases. Fig. 5(a) shows that as the ratio $\frac{\mu_p}{\mu_m}$ increases, d_{33} decreases toward negative values while Fig. 5(b) indicates that as the ratio $\frac{\mu_p}{\mu_m}$ increases, d_{31} increases becomes more positive. Also, Fig. 5 shows that increasing $\frac{\mu_p}{\mu_m}$ to the values greater than 100 or decreasing it to the values less than 0.01 will not have a considerable impact on the value of the effective piezoelectric coefficients. In addition, Fig. 5(a) shows that increasing the ratio $\frac{\epsilon_p}{\epsilon_m}$ from 0.5 to 2 shift d_{33} graph upward and Fig. 5(b) shows that increasing the ratio $\frac{\epsilon_p}{\epsilon_m}$ from 0.5 to 2 shift d_{31} graph downward. This implies that coexistence of elastic mismatch and dielectric mismatch may intensify or weaken the piezoelectric effect. For example, for a composite material composed of a soft inclusion embedded in a hard matrix ($\frac{\mu_p}{\mu_m} \ll 1$), increasing $\frac{\epsilon_p}{\epsilon_m}$ from 0.5 to 0.8 increases d_{33} coefficient and decreases d_{31} coefficient to almost zero. However, if the inclusion is harder than the matrix material ($\frac{\mu_p}{\mu_m} \gg 1$), increasing $\frac{\epsilon_p}{\epsilon_m}$ from 0.5 to 0.8 increases d_{31} coefficient but decreases d_{33} coefficient.

Figs. 6(a) and 6(b) elucidate the effect of dielectric mismatch on the effective d_{31} and d_{33} piezoelectric coefficients, respectively. A sharp dielectric contrast with a very large value of $\frac{\epsilon_p}{\epsilon_m}$ leads to an insignificant piezoelectric effect. Also, these figures show the maximum d_{33} achieved is for a material with $\frac{\epsilon_p}{\epsilon_m} \approx 11$ and soft inclusion in a hard matrix ($\frac{\mu_p}{\mu_m} \leq 10^{-2}$) while the maximum d_{31} piezoelectric coefficient is for hard inclusions embedded in soft matrices where inclusion has small

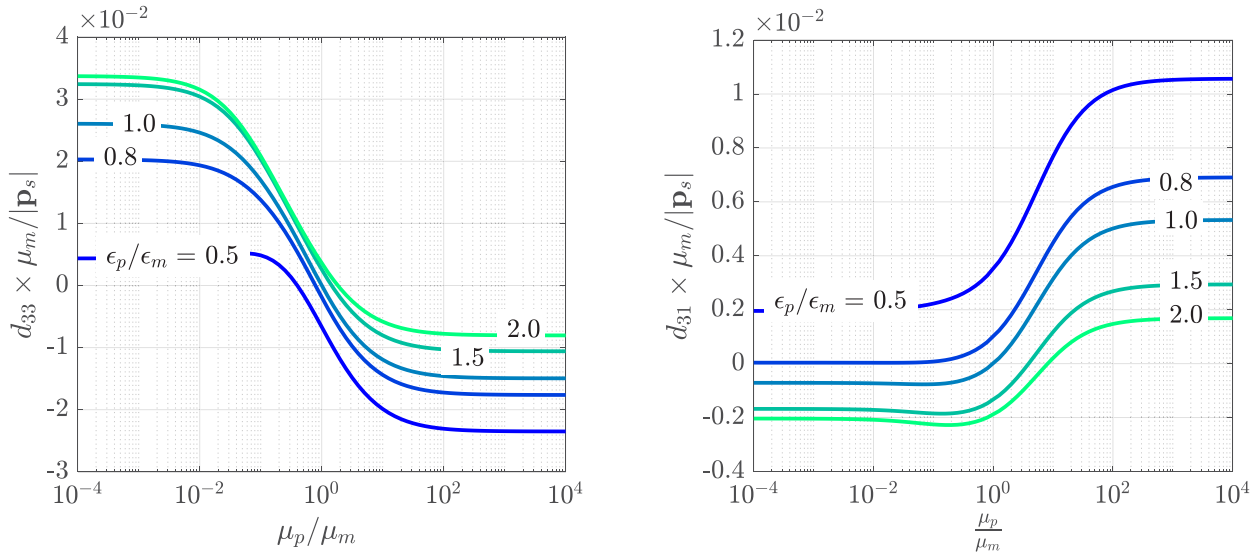

a) Dimensionless effective d_{33} coefficient. b) Dimensionless effective d_{31} coefficient.

Fig. 5. The effect of elastic contrast on the effective (a) d_{33} and (b) d_{31} piezoelectric coefficients.

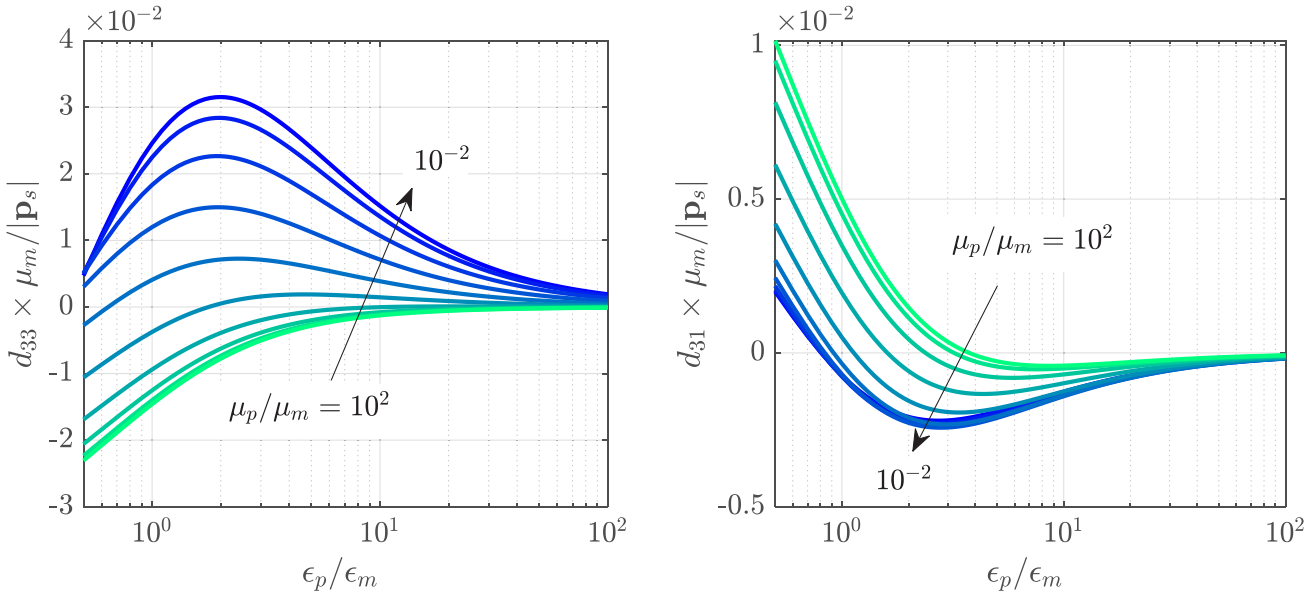

a) Dimensionless effective d_{33} coefficient. b) Dimensionless effective d_{31} coefficient.

Fig. 6. The effect of elastic contrast on the effective (a) d_{33} and (b) d_{31} piezoelectric coefficients.

$\frac{\epsilon_p}{\epsilon_m}$ ratio. Based on Figs. 5 and 6, we can conclude that the material composition that will lead to maximum d_{33} effect is not the same as the material composition that will lead to maximum d_{31} effects. The formulation we presented here can be used to design materials with optimum desirable piezoelectric effect.

The effect of material compressibility on the effective piezoelectric coefficient is studied in Fig. 7. We have set the inclusion Poisson's ratio to $\nu_p = 0.1$ and plotted d_{31} and d_{33} versus volume fraction for different values of matrix Poisson's ratio ν_m in Figs. 7(a) and 7(b), respectively. It is clear that as volume fraction of inclusion increases, piezoelectric coefficients also increase. Also, these figures show that as ν_m increases both d_{31} and d_{33} are improved.

Fig. 8 shows the impact of the spheroid aspect ratio $\frac{a_1}{a_3}$ on the piezoelectric behavior of composite material. We have assumed that the material is composed of a soft inclusion embedded in a hard matrix ($\mu_p/\mu_m = 10^{-3}$). Fig. 8(a) shows that the magnitude of d_{33} piezoelectric coefficient improves with an increase in the aspect ratio unless there is no dielectric mismatch in which case the change in the aspect ratio will not have a significant impact on the piezoelectric coefficient. On the other hand, Fig. 8(b) shows that the d_{31} piezoelectric coefficient remains almost unchanged as the aspect ratio increases. Fig. 8 shows that the d_{33} coefficient can be two to three orders of magnitude larger than d_{31} piezoelectric coefficient. This behavior is consistent with experimental measurement of piezoelectric coefficients of charged polymer foams in which d_{33} coefficient has been reported to be two orders of magnitude greater than the d_{31} coefficient (Neugschwandtner et al., 2001). Based on this figure, we can conclude that one simple way to design a composite material with large d_{33} piezoelectric coefficient is to use spheroid inclusions with large aspect ratios.

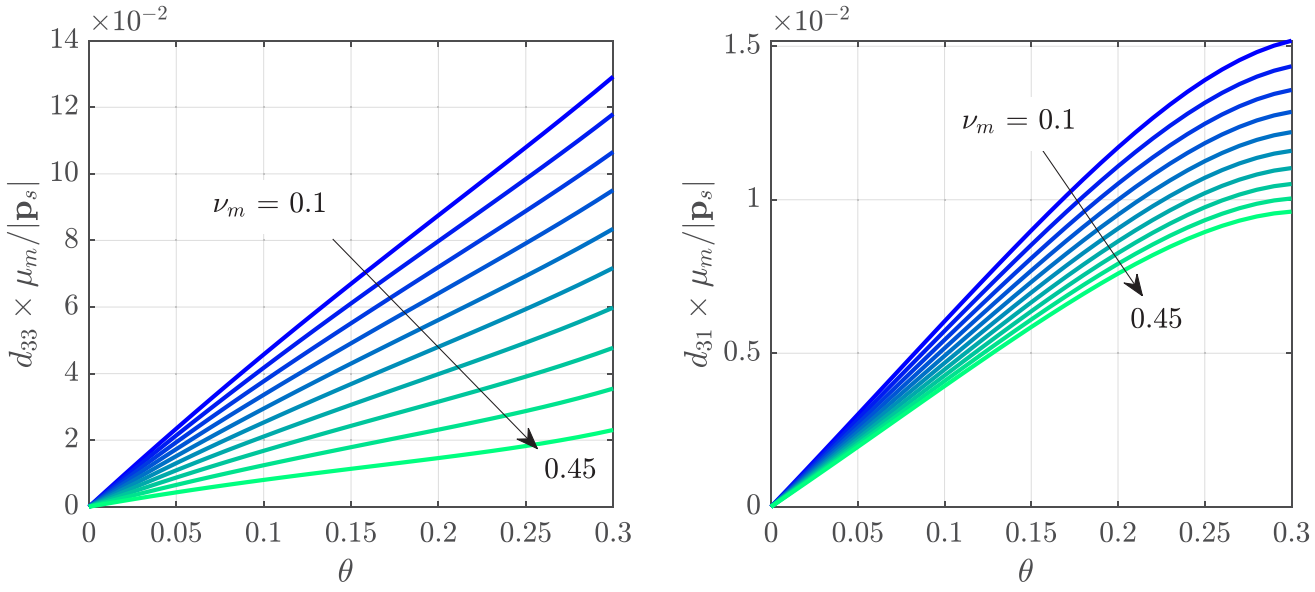

a) Dimensionless effective d_{33} coefficient. b) Dimensionless effective d_{31} coefficient.

Fig. 7. The effect of inclusion volume fraction and the compressibility of the material on the effective (a) d_{33} and (b) d_{31} piezoelectric coefficients ($\frac{\mu_p}{\mu_m} = 10^{-3}$, $\frac{\epsilon_p}{\epsilon_m} = 0.5$, $\nu_p = 0.1$).

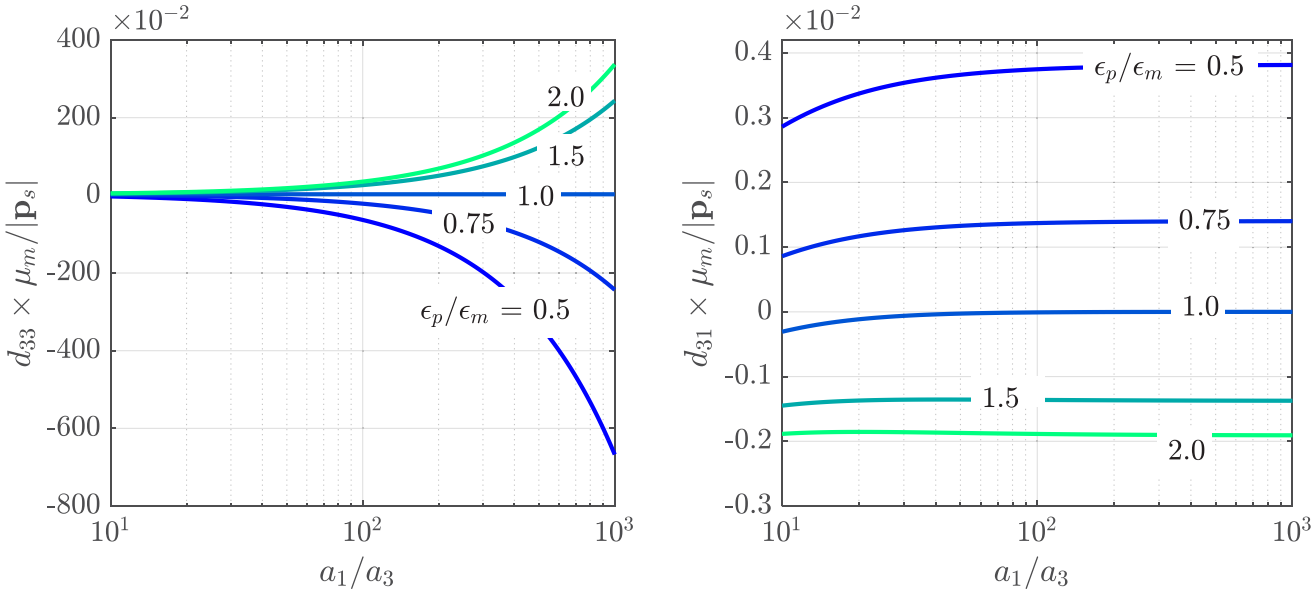

a) Dimensionless effective d_{33} coefficient. b) Dimensionless effective d_{31} coefficient.

Fig. 8. The effect of inclusion aspect ratio on the effective (a) d_{33} and (b) d_{31} piezoelectric coefficients.

The effective piezoelectric coefficient of a composite electret material with spheroid inclusion with $a_1/a_3 = 100$ and $\theta = 0.3$ versus residual polarization $\mathbf{p}_s = p_s\mathbf{e}_3$ has been plotted on Fig. 9. In addition, we have plotted the piezoelectric coefficients of PZT (Guo et al., 2013) and a charged polymer foam electret material (Neugschwandtner et al., 2001). This figure shows that for $p_s \approx 10^{-4}$ C/m^2, both d_{31} and d_{33} coefficients of electret material considered in this work are almost equal to piezoelectric coefficient of charged the PP polymer foam. As the residual polarization increases to $p_s \approx 10^{-2}$, d_{31} piezoelectric coefficient of the electret with spheroid inclusion becomes close to that of a PZT material while d_{33} coefficient of the material considered in this work is two orders of magnitude greater than the piezoelectric coefficient of the PZT. This figure shows that electret material with large residual polarization can exhibit a "giant" piezoelectric effect.

5. Concluding remarks

In summary, we have used the theory of homogenization for soft electrets with charged ellipsoidal inclusions to find the analytical solutions for the emergent piezoelectric response. Our results indicate a subtle interplay between elastic mismatch, dielectric mismatch and microstructure geometry. In particular, our results provide insights into why typical electrets have a rather low d_{31} coefficient and possible approaches to optimize that response (as well as optimize all relevant piezoelectric coefficients). A rather interesting conclusion is that elastic and dielectric mismatch may work against each other. Given our preliminary results, we believe that there is significant scope for all-numerical optimization studies to design next-generation soft materials

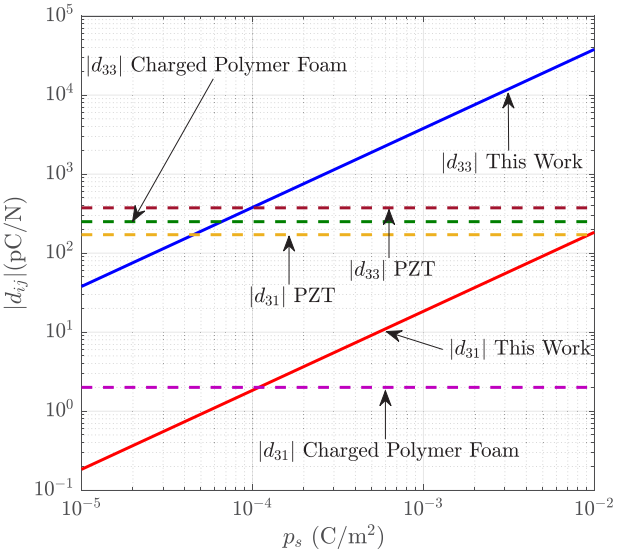

Fig. 9. Comparison of the effective piezoelectric coefficients of electrets with spheroid inclusions with piezoelectric coefficients of PZT (Guo et al., 2013) and charged PP polymer foam (Neugschwandtner et al., 2001).

as done, for instance, in Nanthakumar et al. (2017) and Hamdia et al. (2022).

CRediT authorship contribution statement

Amir Hossein Rahmati: Formal analysis, Investigation, Writing – original draft. **Liping Liu:** Conceptualization, Methodology, Writing – review & editing. **Pradeep Sharma:** Conceptualization, Methodology, Writing – review & editing, Supervision.

Declaration of competing interest

The authors declare that they have no known competing financial interests or personal relationships that could have appeared to influence the work reported in this paper.

Data availability

All data is in the paper.

Appendix. The components of auxiliary Eshelby tensor $\mathbb{S}$ for a unit cell with ellipsoidal inclusion

The integration of Eshelby tensor has been explained in the Eshelby's original paper (Eshelby, 1957) and the textbooks (Li and Wang, 2008; Mura, 2013). We have followed the same approach as explained in the Li and Wang (2008) and calculated component of auxiliary Eshelby tensor $\mathbb{S}$ defined in Eq. (102). The components of $\mathbb{S}$ for an ellipsoidal inclusion is given as

$$\mathbb{S}_{1111} = C_A\left(\frac{C_B}{C_A} - 2\right) I_1 - 3C_A a_1^2 I_{11}, \tag{A.1}$$

$$\mathbb{S}_{1122} = C_A\left(I_1 - a_2^2 I_{12}\right), \tag{A.2}$$

$$\mathbb{S}_{1212} = C_A\left(-\frac{C_B}{2C_A} I_2 - \frac{1}{2}a_1^2 I_{12} - \frac{1}{2}a_2^2 I_{12} + \frac{1}{2} I_1\right), \tag{A.3}$$

$$\mathbb{S}_{1221} = \frac{C_A}{2}\left(I_2 - a_1^2 I_{12} - \frac{C_B}{C_A} I_1 - a_2^2 I_{12}\right), \tag{A.4}$$

where C_A and C_B are constants related to material properties of the matrix material and are defined as

$$C_A = -\frac{1}{a6\pi\mu_m(1-\nu_m)}, \tag{A.5}$$

$$C_B = -\frac{1}{4\pi\mu_m} + \frac{1}{16\pi\mu_m(1-\nu_m)}, \tag{A.6}$$

and $I_{i,j}$ are elliptical integrals defined in Eqs. (58) and (59). All other components of the tensor $\mathbb{S}$ can be obtained by permutation of $(1, 2, 3)$ indices.

References

Abdollahi, A., Domingo, N., Arias, I., Catalan, G., 2019. Converse flexoelectricity yields large piezoresponse force microscopy signals in non-piezoelectric materials. Nature Commun. 10 (1), 1–6.

Alameh, Z., Deng, Q., Liu, L., Sharma, P., 2015. Using electrets to design concurrent magnetoelectricity and piezoelectricity in soft materials. J. Mater. Res. 30 (1), 93–100.

Apte, A., Mozaffari, K., Samghabadi, F.S., Hachtel, J.A., Chang, L., Susarla, S., Idrobo, J.C., Moore, D.C., Glavin, N.R., Litvinov, D., et al., 2020. 2D electrets of ultrathin MoO2 with apparent piezoelectricity. Adv. Mater. 32 (24), 2000006.

Bauer, S., Bauer-Gogonea, S., Dansachmuller, M., Graz, I., Leonhartsberger, H., Salhofer, H., Schwodiauer, R., 2003. Modern electrets. In: IEEE Symposium on Ultrasonics, 2003, Vol. 1. IEEE, pp. 370–376.

Boland, J., Chao, Y.-H., Suzuki, Y., Tai, Y., 2003. Micro electret power generator. In: The Sixteenth Annual International Conference on Micro Electro Mechanical Systems, 2003. MEMS-03 Kyoto. IEEE. IEEE, pp. 538–541.

Cheng, S.-W., Han, T., Huang, T.-Y., Chang Chien, Y.-H., Liu, C.-L., Tang, B.Z., Liou, G.-S., 2018. Novel organic phototransistor-based nonvolatile memory integrated with UV-sensing/green-emissive aggregation enhanced emission (AEE)-active aromatic polyamide electret layer. ACS Appl. Mater. Interfaces 10 (21), 18281–18288.

Cianchetti, M., Laschi, C., Menciassi, A., Dario, P., 2018. Biomedical applications of soft robotics. Nat. Rev. Mater. 3 (6), 143–153.

Cioranescu, D., Donato, P., 1999. An Introduction To Homogenization, Vol. 17. Oxford university press Oxford.

Darbaniyan, F., Dayal, K., Liu, L., Sharma, P., 2019. Designing soft pyroelectric and electrocaloric materials using electrets. Soft Matter 15 (2), 262–277.

Darbaniyan, F., Mozaffari, K., Liu, L., Sharma, P., 2021. Soft matter mechanics and the mechanisms underpinning the infrared vision of snakes. Matter 4 (1), 241–252.

Deng, Q., Liu, L., Sharma, P., 2014a. Electrets in soft materials: Nonlinearity, size effects, and giant electromechanical coupling. Phys. Rev. E 90 (1), 012603.

Deng, Q., Liu, L., Sharma, P., 2014b. Flexoelectricity in soft materials and biological membranes. J. Mech. Phys. Solids 62, 209–227.

Deng, Q., Liu, L., Sharma, P., 2017. A continuum theory of flexoelectricity. In: Flexoelectricity in Solids: From Theory To Applications. World Scientific, pp. 111–167.

Deng, Q., Lv, S., Li, Z., Tan, K., Liang, X., Shen, S., 2020. The impact of flexoelectricity on materials, devices, and physics. J. Appl. Phys. 128 (8), 080902.

Dong, K., Peng, X., Wang, Z.L., 2020. Fiber/fabric-based piezoelectric and triboelectric nanogenerators for flexible/stretchable and wearable electronics and artificial intelligence. Adv. Mater. 32 (5), 1902549.

Eshelby, J.D., 1957. The determination of the elastic field of an ellipsoidal inclusion, and related problems. Proc. R. Soc. Lond. Ser. A Math. Phys. Eng. Sci. 241 (1226), 376–396.

Ghadi, B.M., Yuan, M., Ardebili, H., 2019. Stretchable fabric-based LiCoO2, electrode for lithium ion batteries. Extreme Mech. Lett. 32, 100532.

Gong, S., Zhang, J., Wang, C., Ren, K., Wang, Z.L., 2019. A monocharged electret nanogenerator-based self-powered device for pressure and tactile sensor applications. Adv. Funct. Mater. 29 (41), 1807618.

Grasinger, M., Mozaffari, K., Sharma, P., 2021. Flexoelectricity in soft elastomers and the molecular mechanisms underpinning the design and emergence of giant flexoelectricity. Proc. Natl. Acad. Sci. 118 (21).

Guo, Q., Cao, G., Shen, I., 2013. Measurements of piezoelectric coefficient d33 of lead zirconate titanate thin films using a mini force hammer. J. Vib. Acoust. 135 (1).

Hamdia, K.M., Ghasemi, H., Zhuang, X., Rabczuk, T., 2022. Multilevel Monte Carlo method for topology optimization of flexoelectric composites with uncertain material properties. Eng. Anal. Bound. Elem. 134, 412–418.

Hillenbrand, J., Sessler, G., 2000. Piezoelectricity in cellular electret films. IEEE Trans. Dielectr. Electr. Insul. 7 (4), 537–542.

Hillenbrand, J., Sessler, G., 2008. DC-biased ferroelectrets with large piezoelectric d 33-coefficients. J. Appl. Phys. 103 (7), 074103.

Hiroshi, H., Minoru, T., 1986. Equivalent inclusion method for steady state heat conduction in composites. Internat. J. Engrg. Sci. 24 (7), 1159–1172.

Kacprzyk, R., Dobrucki, A., Gajewski, J., 1997. Double-layer electret transducer. J. Electrost. 39 (1), 33–40.

Kammoun, M., Berg, S., Ardebili, H., 2016. Stretchable spiral thin-film battery capable of out-of-plane deformation. J. Power Sources 332, 406–412.

Kashiwagi, K., Okano, K., Miyajima, T., Sera, Y., Tanabe, N., Morizawa, Y., Suzuki, Y., 2011. Nano-cluster-enhanced high-performance perfluoro-polymer electrets for energy harvesting. J. Micromech. Microeng. 21 (12), 125016.

Kim, D.-H., Lu, N., Huang, Y., Rogers, J.A., 2012. Materials for stretchable electronics in bioinspired and biointegrated devices. MRS Bull. 37 (3), 226–235.

Krichen, S., Sharma, P., 2016. Flexoelectricity: A perspective on an unusual electromechanical coupling. J. Appl. Mech. 83 (3).
Lakes, R., 2015. Third-rank piezoelectricity in isotropic chiral solids. Appl. Phys. Lett. 106 (21), 212905.
Lakes, R., 2016. Static and dynamic effects of chirality in dielectric media. Modern Phys. Lett. B 30 (24), 1650319.
Lefevre, V., Lopez-Pamies, O., 2017. Homogenization of elastic dielectric composites with rapidly oscillating passive and active source terms. SIAM J. Appl. Math. 77 (6), 1962–1988.
Li, S., Wang, G., 2008. Introduction To Micromechanics and Nanomechanics. World Scientific Publishing Company.
Lim, H.-R., Kim, H.S., Qazi, R., Kwon, Y.-T., Jeong, J.-W., Yeo, W.-H., 2020. Advanced soft materials, sensor integrations, and applications of wearable flexible hybrid electronics in healthcare, energy, and environment. Adv. Mater. 32 (15), 1901924.
Liu, L., 2008. Solutions to the eshelby conjectures. Proc. R. Soc. Lond. Ser. A Math. Phys. Eng. Sci. 464 (2091), 573–594.
Liu, L., 2014. An energy formulation of continuum magneto-electro-elasticity with applications. J. Mech. Phys. Solids 63, 451–480.
Liu, L., Sharma, P., 2018. Emergent electromechanical coupling of electrets and some exact relations—The effective properties of soft materials with embedded external charges and dipoles. J. Mech. Phys. Solids 112, 1–24.
Luo, A., Xu, Y., Zhang, Y., Zhang, M., Zhang, X., Lu, Y., Wang, F., 2021. Spray-coated electret materials with enhanced stability in a harsh environment for an MEMS energy harvesting device. Microsyst. Nanoeng. 7 (1), 1–9.
Majdoub, M., Sharma, P., Cagin, T., 2008. Enhanced size-dependent piezoelectricity and elasticity in nanostructures due to the flexoelectric effect. Phys. Rev. B 77 (12), 125424.
Majdoub, M., Sharma, P., Çağin, T., 2009. Erratum: Enhanced size-dependent piezoelectricity and elasticity in nanostructures due to the flexoelectric effect [Phys. Rev. B 77, 125424 (2008)]. Phys. Rev. B 79 (11), 119904.
Mbarki, R., Baccam, N., Dayal, K., Sharma, P., 2014. Piezoelectricity above the Curie temperature? Combining flexoelectricity and functional grading to enable high-temperature electromechanical coupling. Appl. Phys. Lett. 104 (12), 122904.
Milton, G., 2002. The Theory of Composites. In: Cambridge Monographs on Applied and Computational Mathematics, Cambridge University Press, Cambridge, UK.
Mocci, A., Barceló-Mercader, J., Codony, D., Arias, I., 2021. Geometrically polarized architected dielectrics with apparent piezoelectricity. J. Mech. Phys. Solids 157, 104643.
Mohammadi, P., Liu, L., Sharma, P., 2014. A theory of flexoelectric membranes and effective properties of heterogeneous membranes. J. Appl. Mech. 81 (1).
Mura, T., 2013. Micromechanics of Defects in Solids. Springer Science & Business Media.
Nanthakumar, S., Zhuang, X., Park, H.S., Rabczuk, T., 2017. Topology optimization of flexoelectric structures. J. Mech. Phys. Solids 105, 217–234.
Neugschwandtner, G., Schwödiauer, R., Bauer-Gogonea, S., Bauer, S., 2000. Large piezoelectric effects in charged, heterogeneous fluoropolymer electrets. Appl. Phys. A 70 (1), 1–4.
Neugschwandtner, G.S., Schwödiauer, R., Bauer-Gogonea, S., Bauer, S., Paajanen, M., Lekkala, J., 2001. Piezo-and pyroelectricity of a polymer-foam space-charge electret. J. Appl. Phys. 89 (8), 4503–4511.
Newnham, R., Sundar, V., Yimnirun, R., Su, J., Zhang, Q., 1997. Electrostriction: nonlinear electromechanical coupling in solid dielectrics. J. Phys. Chem. B 101 (48), 10141–10150.
Nguyen, T.D., Mao, S., Yeh, Y.-W., Purohit, P.K., McAlpine, M.C., 2013. Nanoscale flexoelectricity. Adv. Mater. 25 (7), 946–974.
Qu, S., Yu, Y., 2011. Electromechanical coupling properties and stability analysis of ferroelectrets. J. Appl. Phys. 110 (4), 043525.
Rafsanjani, A., Zhang, Y., Liu, B., Rubinstein, S.M., Bertoldi, K., 2018. Kirigami skins make a simple soft actuator crawl. Science Robotics 3 (15), eaar7555.
Rahmati, A.H., Bauer, S., Yang, S., Sharma, P., 2019. Nonlinear bending deformation of soft electrets and prospects for engineering flexoelectricity and transverse (d_{31}) piezoelectricity. Soft Matter 15 (1), 127–148.
Rogers, J.A., Someya, T., Huang, Y., 2010. Materials and mechanics for stretchable electronics. Science 327 (5973), 1603–1607.
Rosenkilde, C.E., 1967. Surface-energy tensors for ellipsoids. J. Math. Phys. 8 (1), 88–97.
Sessler, G.M., 1980. Physical principles of electrets. Electrets 13–80.
Sessler, G., Hillenbrand, J., 1999. Electromechanical response of cellular electret films. In: 10th International Symposium on Electrets (ISE 10). Proceedings (Cat. No. 99 CH36256). IEEE, pp. 261–264.
Sessler, G.M., West, J.E., 1966. Foil-electret microphones. J. Acoust. Soc. Am. 40 (6), 1433–1440.
Sharma, P., 2004. Size-dependent elastic fields of embedded inclusions in isotropic chiral solids. Int. J. Solids Struct. 41 (22–23), 6317–6333.
Sharma, P., Dasgupta, A., 2002. Average elastic fields and scale-dependent overall properties of heterogeneous micropolar materials containing spherical and cylindrical inhomogeneities. Phys. Rev. B 66 (22), 224110.
Sharma, N., Maranganti, R., Sharma, P., 2007. On the possibility of piezoelectric nanocomposites without using piezoelectric materials. J. Mech. Phys. Solids 55 (11), 2328–2350.
Suzuki, Y., Miki, D., Edamoto, M., Honzumi, M., 2010. A MEMS electret generator with electrostatic levitation for vibration-driven energy-harvesting applications. J. Micromech. Microeng. 20 (10), 104002.
Tagantsev, A.K., Yudin, P.V., 2016. Flexoelectricity in Solids: From Theory To Applications. World Scientific.
Tan, K., Wen, X., Deng, Q., Shen, S., Liu, L., Sharma, P., 2021. Soft rubber as a magnetoelectric material—Generating electricity from the remote action of a magnetic field. Mater. Today 43, 8–16.
Tian, L., 2008. Effective Behavior of Dielectric Elastomer Composites (Ph.D. thesis). California Institute of Technology.
Tian, L., Tevet-Deree, L., DeBotton, G., Bhattacharya, K., 2012. Dielectric elastomer composites. J. Mech. Phys. Solids 60 (1), 181–198.
Torbati, M., Mozaffari, K., Liu, L., Sharma, P., 2022. Coupling of mechanical deformation and electromagnetic fields in biological cells. Rev. Modern Phys. 94 (2), 025003.
Trivedi, D., Rahn, C.D., Kier, W.M., Walker, I.D., 2008. Soft robotics: Biological inspiration, state of the art, and future research. Appl. Bionics Biomech. 5 (3), 99–117.
Wang, B., Yang, S., Sharma, P., 2019. Flexoelectricity as a universal mechanism for energy harvesting from crumpling of thin sheets. Phys. Rev. B 100 (3), 035438.
Wen, X., Li, D., Tan, K., Deng, Q., Shen, S., 2019. Flexoelectret: an electret with a tunable flexoelectriclike response. Phys. Rev. Lett. 122 (14), 148001.
Yang, L., Dayal, K., 2011. A completely iterative method for the infinite domain electrostatic problem with nonlinear dielectric media. J. Comput. Phys. 230 (21), 7821–7829.
Yang, S., Zhao, X., Sharma, P., 2017. Avoiding the pull-in instability of a dielectric elastomer film and the potential for increased actuation and energy harvesting. Soft Matter 13 (26), 4552–4558.
Yudin, P., Tagantsev, A., 2013. Fundamentals of flexoelectricity in solids. Nanotechnology 24 (43), 432001.
Zhang, X., Hillenbrand, J., Sessler, G.M., 2004. Piezoelectric d 33 coefficient of cellular polypropylene subjected to expansion by pressure treatment. Appl. Phys. Lett. 85 (7), 1226–1228.
Zhang, M., Yan, D., Wang, J., Shao, L.-H., 2021. Ultrahigh flexoelectric effect of 3D interconnected porous polymers: modelling and verification. J. Mech. Phys. Solids 151, 104396.
Zhao, X., Suo, Z., 2008. Electrostriction in elastic dielectrics undergoing large deformation. J. Appl. Phys. 104 (12), 123530.
Zhuang, X., Nguyen, B.H., Nanthakumar, S.S., Javvaji, B., Tran, T.Q., 2022. Computational modelling of flexoelectricity: State-of-the-art and challenges. In: Current Trends and Open Problems in Computational Mechanics. Springer, pp. 593–606.
Zubko, P., Catalan, G., Tagantsev, A.K., 2013. Flexoelectric effect in solids. Annu. Rev. Mater. Res. 43, 387–421.